SIAM J. Applied Dynamical Systems
Vol. 15, No. 4, pp. 2017–2050

Self-Similar Solutions for Reversing Interfaces in the Slow Diffusion Equation with Strong Absorption*

Jamie M. Foster† and Dmitry E. Pelinovsky‡

Abstract. We consider the slow nonlinear diffusion equation subject to a strong absorption rate and construct local self-similar solutions for reversing (and antireversing) interfaces, where an initially advancing (receding) interface gives way to a receding (advancing) one. We use an approach based on invariant manifolds, which allows us to determine the required asymptotic behavior for small and large values of the concentration. We then "connect" the requisite asymptotic behaviors using a robust and accurate numerical scheme. By doing so, we are able to furnish a rich set of self-similar solutions for both reversing and antireversing interfaces. The stability of these self-similar solutions is validated against direct numerical simulation in the case of constant absorption.

Key words. nonlinear diffusion equation, slow diffusion, strong absorption, self-similar solutions, invariant manifolds, reversing interface, antireversing interface

AMS subject classifications. 35K55, 37C70, 76R50

DOI. 10.1137/15M1039006

1. Introduction.

We address reversing and antireversing properties of interfaces in the following one-dimensional slow diffusion equation with absorption,

$$\frac{\partial h}{\partial t} = \frac{\partial}{\partial x}\left(h^m \frac{\partial h}{\partial x}\right) - h^n, \tag{1.1}$$

where h is a positive function on a compact support, e.g., a concentration of some species, and x and t denote space and time, respectively. Restricting the exponents to the ranges $m > 0$ and $n < 1$ corresponds to slow diffusion and strong absorption, respectively. We emphasize that the nonlinear diffusion equation (1.1) is defined on a compact, time-dependent spatial domain, subject to appropriate conditions at the moving interfaces (or free boundaries) of the spatial domain.

Interfaces correspond to the points on the x-axis where regions for positive solutions for h are connected with the regions where h is identically zero. The initial condition $h|_{t=0} = h_0$ is assumed to be compactly supported and strictly positive inside the compact support. The

*Received by the editors September 9, 2015; accepted for publication (in revised form) by M. Pugh August 18, 2016; published electronically November 1, 2016.
http://www.siam.org/journals/siads/15-4/M103900.html
Funding: The work of the first author was supported by a postdoctoral fellowship at McMaster University. The work of the second author was supported by the Ministry of Education and Science of Russian Federation (the base part of the State task 2014/133, project 2839).
†Department of Mathematics, University of Portsmouth, Winston Churchill Avenue, Portsmouth, England, PO1 2UP (jamie.foster@port.ac.uk).
‡Department of Mathematics, McMaster University, 1280 Main Street West, Hamilton, Ontario, Canada, L8S 4K1 and Department of Applied Mathematics, Nizhny Novgorod State Technical University, 24 Minin Street, Nizhny Novgorod, 603950, Russia (dmpeli@math.mcmaster.ca).

motion of the interfaces is determined from conditions [8] that require the function h be continuous (i.e., vanishing at the interface) and the flux of h through the interface to be zero; see conditions (1.2) or (1.3) below.

We note the contrasting terminology used here and in the fluid dynamics literature. Most fluid dynamicists use the term "interface" for the free surface of a fluid (i.e., the air-liquid interface), whereas the term "contact line" would typically be used to refer to the triple junction where the air, liquid, and substrate all meet.

The slow diffusion equation with strong absorption (1.1) describes a variety of different physical processes, including (i) the slow spreading of a slender viscous film over a horizontal plate subject to the action of gravity and a constant evaporation rate [1] (when $m = 3$ and $n = 0$); (ii) the dispersion of a biological population subject to a constant death rate [10] (when $m = 2$ and $n = 0$); (iii) nonlinear heat conduction along a rod with a constant rate of heat loss [11] (when $m = 4$ and $n = 0$); (iv) and fluid flows in porous media with a drainage rate driven by gravity or background flows [2, 16] (when $m = 1$ and either $n = 1$ or $n = 0$).

In the presence of slow diffusion ($m > 0$), the interfaces of compactly supported solutions have a finite propagation speed [11]. In the presence of strong absorption ($0 < n < 1$), the solution vanishes for all x after some finite time, which is referred to as finite-time extinction [13, 15]. Therefore, the interfaces for compactly supported initial data coalesce in a finite time. Depending on the shape of h_0 and the values of m and n, the interfaces may change their direction of propagation in a number of different ways. It was proved by Chen, Matano, and Mimura [3] that bell-shaped initial data remain bell shaped for all time before the compact support shrinks to a point. However, the possible types of dynamics of interfaces for this bell-shaped data were not identified in [3].

Let us denote the location of the left interface by $x = \ell(t)$ and the limit $x \searrow \ell(t)$, where h is nonzero, by $x = \ell(t)^+$. If $m > 0$, $0 < n < 1$, and $m + n \geq 1$, it was proved in [8] that the position of the interface, $\ell(t)$, is a Lipschitz continuous function of time. In the case $m + n = 1$, the function $\ell(t)$ is found from the boundary conditions $h|_{x=\ell(t)} = 0$ and

$$\frac{d\ell}{dt} = -h^{m-1}\frac{\partial h}{\partial x}\Big|_{x=\ell(t)^+} + \left(h^{m-1}\frac{\partial h}{\partial x}\Big|_{x=\ell(t)^+}\right)^{-1}. \tag{1.2}$$

In the case $m + n > 1$, the spatial derivatives at $x = \ell(t)^+$ are not well defined [8] and the zero flux condition (1.2) must be written as

$$\frac{d\ell}{dt} = \begin{cases} -h^{m-1}\frac{\partial h}{\partial x}\Big|_{x=\ell(t)^+} & \text{if } \ell' \leq 0, \\ h^n\left(\frac{\partial h}{\partial x}\right)^{-1}\Big|_{x=\ell(t)^+} & \text{if } \ell' \geq 0, \end{cases} \tag{1.3}$$

where a prime denotes differentiation with respect to time.

The analysis of [15, 3, 8] on weak solutions to the slow diffusion equation (1.1) was restricted to the range $0 < n < 1$, in which case the zero solution satisfies (1.1) on the infinite line. Weak formulation of the slow diffusion equation (1.1) was also considered in the range $1 - m < n \leq 0$ (for $m > 1$) in [14], where existence of weak solutions was proven for the

modified equation

$$\frac{\partial h}{\partial t} = \frac{\partial}{\partial x}\left(h^m \frac{\partial h}{\partial x}\right) - h^n \chi_{\{h>0\}}. \tag{1.4}$$

The modification involves the characteristic function χ and is included to ensure that the zero solution satisfies (1.4) on the infinite line. Under suitable conditions on the initial data, weak solutions to (1.4) were constructed and it was proven in [14] that the weak solutions are classical at the points (x,t), for which h is positive. It is our understanding that the work of [3, 8] can be applied to the modified equation (1.4) with $1-m<n\leq 0$ verbatim, so that the positive solution of the slow diffusion equation (1.1) with $m>0$, $n<1$, and $m+n>1$ can be closed at the left interface $x=\ell(t)$ subject to the interface equation (1.3).

One could choose to close the slow diffusion equation (1.1) on a compact interval in a variety of ways, e.g., by supplying analogous conditions at the right interface, or by supplying a Dirichlet or Neumann condition at a symmetry point. For instance, if h_0 is even in x, then the solution h remains even in x for all times and, therefore, the slow diffusion equation (1.1) can be closed on the compact interval $[\ell(t),0]$ by imposing $\partial h/\partial x|_{x=0}=0$. However, such details do not concern us here because we are interested in studying the behavior of solutions to (1.1) local to the left interface $x=\ell(t)$ only.

We reiterate further the main question of this work on the possible types of dynamics in the slow diffusion equation with strong absorption (1.1). Working with bell-shaped, compactly supported initial data h_0, one can anticipate a priori that the compact support of the bell-shaped solution can either (i) decrease monotonically in time, (ii) first expand and then subsequently shrink, (iii) or have more complicated behavior where multiple instances of expansion and contraction are observed. This phenomenon brings about both "reversing" and "antireversing" dynamics of an interface. Here the term reversing describes a scenario where the velocity of the left interface $x=\ell(t)$ satisfies $\ell'(t)<0$ before the reversing time and $\ell'(t)>0$ after the reversing time, whereas the term antireversing refers to the opposite scenario with $\ell'(t)>0$ before and $\ell'(t)<0$ after the reversing time.

The first analytical solution to (1.1) exhibiting a reversing interface was obtained by Kersner [15] for the case $m+n=1$. This explicit solution takes the form

$$u^m(x,t) = \frac{m}{2(m+1)(m+2)t}\left[Ct^{\frac{2}{m+2}} - (m+2)^2t^2 - x^2\right]_+, \tag{1.5}$$

where the plus subscript denotes the positive part of the function, and $C>0$ is an arbitrary parameter. The interfaces are located symmetrically at $x=\pm\ell(t)$ with

$$\ell(t) = \sqrt{Ct^{\frac{2}{m+2}} - (m+2)^2t^2}. \tag{1.6}$$

More recently, Foster et al. [6] considered the case $m+n>1$ and explored the asymptotic and numerical construction of self-similar solutions for (1.1)—some related, yet different, self-similar solutions to other nonlinear diffusion equations have previously been constructed using a combination of asymptotic analysis and numerical shooting; see, e.g., [7, 19].

The self-similar solutions capture the relevant dynamics of reversing interfaces near the corresponding points in space and time (which can be placed at the origin of x and t without

the loss of generality). Based on a classical point symmetry analysis of the porous medium equation (1.1)—provided in [9]—the authors of [6] found that reversing interfaces can be described via the self-similar reductions

$$h(x,t) = (\pm t)^{\frac{1}{1-n}} \; H_\pm(\xi), \quad \xi = x(\pm t)^{-\frac{m+1-n}{2(1-n)}}, \quad \pm t > 0, \tag{1.7}$$

where the functions $H_\pm$ satisfy the following pair of second-order differential equations:

$$\frac{d}{d\xi}\left(H_\pm^m \frac{dH_\pm}{d\xi}\right) \pm \frac{m+1-n}{2(1-n)}\,\xi \frac{dH_\pm}{d\xi} = H_\pm^n \pm \frac{1}{1-n} H_\pm, \tag{1.8}$$

where $m > 0$, $n < 1$, and $m + n > 1$ is assumed in what follows.

We seek positive solutions $H_\pm$ of the differential equations (1.8) on the semi-infinite line $[A_\pm, \infty)$ that satisfy the following conditions:

$$\text{(i)} \quad H_\pm(\xi) \to 0 \quad \text{as} \quad \xi \to A_\pm, \tag{1.9}$$

$$\text{(ii)} \quad H_\pm(\xi) \text{ is monotonically increasing for all } \xi > A_\pm, \tag{1.10}$$

$$\text{(iii)} \quad H_\pm(\xi) \to +\infty \quad \text{as} \quad \xi \to +\infty. \tag{1.11}$$

The first of these conditions, (1.9), are the self-similar counterparts of the condition $h|_{x=\ell(t)} = 0$ for (1.1). In addition, the behavior of $H_-(\xi)$ and $H_+(\xi)$ in the far field must be matched from the condition

$$\lim_{\xi\to\infty} \frac{H_+(\xi)}{H_-(\xi)} = 1. \tag{1.12}$$

The requirement (1.12) is tantamount to enforcing that the solution h to the slow diffusion equation (1.1) does not "jump" as t passes through zero—this can be verified by taking both the limits $t \searrow 0$ and $t \nearrow 0$ in the self-similar reduction (1.7).

Existence of solutions to the differential equations (1.8) on $[A_\pm, \infty)$ with the required behavior (1.12) implies, via the self-similar reduction (1.7), the existence of a reversing (if $A_\pm > 0$) or antireversing (if $A_\pm < 0$) left interface at $x = \ell(t)$, which behaves like

$$\ell(t) = A_\pm(\pm t)^{\frac{m+1-n}{2(1-n)}}, \quad \pm t > 0, \tag{1.13}$$

after placing the reversing point at the origin of the space-time plane. If $m + n > 1$, the velocity of the interface, given by $\ell'(t)$, changes sign continuously as t passes through zero.

By combining formal asymptotic constructions of the solutions $H_\pm$ near the small and large values with a numerical shooting method, the authors of [6] claimed that for $n = 0$ and for integer values of $m = 2, 3, 4$, there exists a unique positive value of A_-, which leads to a monotonically growing function H_- on the entire semiaxis $[A_-, \infty)$. Using the far-field matching condition (1.12), a unique, monotonically growing function H_+ is found on $[A_+, \infty)$ for a positive value of A_+. These solutions correspond to a reversing left interface $x = \ell(t)$. No solutions exhibiting an antireversing interface were found in [6].

In the present work, we address the same problem using a dynamical system framework [12, 18]. The dynamical system theory allows us to justify the formal asymptotic approximations

of $H_\pm$ for small and large values, as well as to set up an accurate and robust numerical procedure for furnishing appropriate solutions to the differential equations (1.8). Qualitatively, we recover the results of [6] for $n = 0$ and $m = 3, 4$, but with better precision, and we generalize these results for all noninteger values of $m > 0$, $n < 1$, and $m + n > 1$. In addition, we demonstrate that the result for $n = 0$ and $m = 2$, reported in [6], is incorrect and no self-similar reversing interface solutions exist in this case. Finally, we discover new reversing and antireversing interface solutions of the same differential equations (1.8) for other values of m when $n = 0$.

Our approach explores invariant manifolds for the singular differential equations after appropriate unfolding (which is sometimes referred to as the blow-up technique [5, 17]). The main analytical results of this work are given by the following theorems.

Theorem 1.1. *For every $m > 0$, $n < 1$, $m + n > 1$ and for every $A_\pm \neq 0$, there exists a unique solution of the differential equations (1.8) such that $H_\pm(\xi) \to 0$ as $\xi \to A_\pm$. If $\pm A_\pm > 0$, this unique solution has the following asymptotic behavior,*

$$H_\pm(\xi) = \left[\pm\frac{2(1-n)^2}{(m+1-n)A_\pm}(\xi - A_\pm)\right]^{1/(1-n)} \left[1 + \mathcal{O}\left((\xi - A_\pm)^\kappa\right)\right] \quad \text{as} \quad \xi \to A_\pm, \tag{1.14}$$

with $\kappa := \min\{1, (m+n-1)/(1-n)\}$, whereas if $\pm A_\pm < 0$, it has the following asymptotic behavior,

$$H_\pm(\xi) = \left(\mp\frac{m(m+1-n)A_\pm}{2(1-n)}(\xi - A_\pm)\right)^{1/m} \left[1 + \mathcal{O}\left((\xi - A_\pm)^{\frac{m+n-1}{m}}\right)\right] \text{ as } \xi \to A_\pm. \tag{1.15}$$

Theorem 1.2. *For every $m > 0$, $n < 1$, and $m + n > 1$, there exists a one-parameter family of solutions of the differential equation (1.8) for the lower sign such that $H_-(\xi) \to +\infty$ as $\xi \to +\infty$, and this family has the following asymptotic behavior,*

$$H_-(\xi) \sim \left(\frac{\xi}{x_0}\right)^{\frac{2}{m+1-n}} \quad \text{as} \quad \xi \to +\infty, \tag{1.16}$$

where $x_0 > 0$ is an arbitrary parameter. There exists a two-parameter family of solutions of the differential equation (1.8) for the upper sign such that $H_+(\xi) \to +\infty$ as $\xi \to +\infty$, and this family has the same asymptotic behavior (1.16) for some $x_0 > 0$.

The main problem is to connect the two asymptotic behaviors of the differential equations (1.8) which are defined for small and large values of $H_\pm$ by Theorems 1.1 and 1.2. We know from [6] that there exists an exact solution of the connection problem if $A_\pm = 0$. This exact solution is given by

$$H_\pm(\xi) = \left(\frac{(m+1-n)^2}{2(m+n+1)}\xi^2\right)^{\frac{1}{m+1-n}}, \quad \xi \in (0, \infty). \tag{1.17}$$

However, the exact profile (1.17) corresponds to a solution to the slow diffusion equation (1.1) with an interface that remains stationary for all time, thus we do not examine it further here.

Some connection results for nonzero values of $A_\pm$ are available for the differential equations (1.8) in Lemmas 4.1 and 4.4 below. Although these results are not sufficient for an analytical solution of the connection problem, we can set up a numerical method, which detects connections of the two solutions described in Theorems 1.1 and 1.2.

We emphasize in passing that the asymptotic behavior of the self-similar solutions $H_\pm$ constructed in Theorem 1.1 coincide with the interface conditions (1.3). For simplicity, we consider the reversing event with $A_\pm > 0$. For $\ell'(t) > 0$, $t > 0$, we use (1.3), (1.7), and (1.14) to obtain

$$\frac{d\ell}{dt} = \lim_{x\to\ell(t)^+} h^n \left(\frac{\partial h}{\partial t}\right)^{-1} = t^{\frac{m+1-n}{2(1-n)}-1} \lim_{\xi\to A_+^+} H_+^n \left(\frac{H_+}{d\xi}\right)^{-1} = \frac{m+1-n}{2(1-n)} A_+ t^{\frac{m+1-n}{2(1-n)}-1}. \tag{1.18}$$

This equation matches with the interface equation (1.13). Similarly, for $\ell'(t) < 0$, $t < 0$, we use (1.3), (1.7), and (1.15) to obtain

$$\frac{d\ell}{dt} = -\lim_{x\to\ell(t)^+} h^{m-1}\frac{\partial h}{\partial t} = t^{\frac{m+1-n}{2(1-n)}-1} \lim_{\xi\to A_-^+} H_-^{m-1}\frac{H_-}{d\xi} = \frac{m+1-n}{2(1-n)} A_- t^{\frac{m+1-n}{2(1-n)}-1}. \tag{1.19}$$

This equation matches again with the interface equation (1.13). Thus, the self-similar solutions constructed in this work satisfy the weak formulation of solutions to the slow diffusion equation with strong absorption constructed in [3, 8, 14].

The remainder of the paper is organized as follows. The unfolding and invariant manifolds for the differential equations (1.8) near small values of $H_\pm$ are described in section 2. The corresponding results near large values of $H_\pm$ are reported in section 3. Theorems 1.1 and 1.2 are proved in these two sections. The connection problem between the invariant manifolds near small and large values of $H_\pm$ is considered in section 4. The relevant numerical technique is implemented in section 5, where the main findings are discussed for $n = 0$ and compared with the previous results from [6]. In section 6, we carry out direct numerical simulation of (1.1) to provide numerical evidence of the relevance of the self-similar solutions to the dynamics of (1.1) in the case $n = 0$. Finally, the summary of this work is provided in the concluding section 7.

2. Invariant manifolds for small values of $H_\pm$. We shall rewrite the scalar equations (1.8) as vector systems for variables $u = H_\pm$ and $w = H_\pm^m dH_\pm/d\xi$. In the interests of simplicity of notation, we drop the plus and minus subscripts in the definitions of the variables u and w. The nonautonomous vector system for u and w is as follows:

$$\frac{du}{d\xi} = \frac{w}{u^m} \tag{2.1}$$

and

$$\frac{dw}{d\xi} = u^n \pm \frac{1}{1-n} u \mp \frac{m+1-n}{2(1-n)} \frac{\xi w}{u^m}. \tag{2.2}$$

If m and n are nonintegers, we require the constraint $u \geq 0$. In either case, only positive solutions for u need to be considered.

The interface, in self-similar variables, is assumed to be located at $\xi = A \in \mathbb{R}$, where $u = 0$—a requirement of the condition on the continuity of $h(x,t)$ at $x = \ell(t)$. Since the value $u = 0$ is singular in the nonautonomous system (2.1), we shall unfold the singularity by introducing a convenient parameterization of solutions with a new time variable τ defined by

$$\frac{d\xi}{d\tau} = u^m, \quad u \geq 0. \tag{2.3}$$

The map $\tau \mapsto \xi$ is increasing and if $\xi \to A$ as $\tau \to -\infty$, then $\xi > A$ for finite values of τ.

With the parameterization $\tau \mapsto \xi$, we obtain the autonomous dynamical system in $\mathbb{R}^3$,

$$\left\{ \begin{array}{l} \dot{\xi} = u^m, \\ \dot{u} = w, \\ \dot{w} = u^{m+n} \pm \frac{1}{1-n} u^{m+1} \mp \frac{m+1-n}{2(1-n)} \xi w, \end{array} \right. \tag{2.4}$$

where the dots stand for the derivatives of (ξ, u, w) in τ. The last two equations of system (2.4) are continuously differentiable near zero values of u because $m > 0$, $n < 1$, and $m + n > 1$. If $m \in (0,1)$, the first equation of system (2.4) is not continuously differentiable at $u = 0$, but this singularity is induced by the parameterization of the map $\tau \mapsto \xi$ defined by (2.3).

The family of equilibrium points for the system (2.4) is given by $(\xi, u, w) = (A, 0, 0)$, where $A \in \mathbb{R}$ is an arbitrary parameter. If $m > 1$, each equilibrium point is associated with the Jacobian matrix

$$\left[\begin{array}{ccc} 0 & 0 & 0 \\ 0 & 0 & 1 \\ 0 & 0 & \mp \frac{m+1-n}{2(1-n)} A \end{array} \right].$$

This Jacobian matrix has a double zero eigenvalue (with two linearly independent eigenvectors) and a simple nonzero eigenvalue $\mp A(m+1-n)/(2-2n)$. Therefore, the linearization of the dynamical system (2.4) at the equilibrium point $(A,0,0)$ with $\pm A > 0$ has a two-dimensional center manifold and a one-dimensional stable manifold, whereas the linearized system with $\pm A < 0$ has a two-dimensional center manifold and a one-dimensional unstable manifold.

If $m > 1$, $n < 1$, and $m + n > 1$, the dynamical system (2.4) is C^1 smooth, so that a straightforward application of the invariant manifold theorems [12, 18] asserts that the equilibrium point $(A,0,0)$ with $A \neq 0$ is located at the intersection of the two invariant manifolds, which are tangential to the invariant manifolds of the linearized system. The limited smoothness of the first equation in system (2.4) for $m \in (0,1)$ can also be incorporated into analysis. We formulate the corresponding results in the following Propositions 2.1 and 2.2. The relevant conclusions on the behavior of solutions of the differential equations (1.8) for small values of $H_\pm$, expressed in Theorem 1.1, follow from these two propositions.

Proposition 2.1. *For every $m > 0$, $n < 1$, and $m + n > 1$ and for every $A \neq 0$, there exists a two-dimensional center manifold of the dynamical system (2.4) near the equilibrium point $(A,0,0)$, which can be parameterized as follows:*

$$W_c(A,0,0) = \left\{ w = u^{m+n} \eta(\xi, u), \ \ \xi \in (A, A+\delta), \ \ u \in (0, \delta) \right\}, \tag{2.5}$$

where

$$\eta(\xi, u) = \pm \frac{2(1-n)}{(m+1-n)A} + \mathcal{O}(\xi - A, u^{\min\{1-n, m+n-1\}}) \tag{2.6}$$

and $\delta > 0$ is small. Dynamics of the system (2.4) on the center manifold $W_c(A,0,0)$ is topologically equivalent to the dynamics at the truncated normal form

$$\begin{cases} \dot{\xi} = u^m, \\ \dot{u} = \pm \frac{2(1-n)u^{m+n}}{(m+1-n)A}. \end{cases} \tag{2.7}$$

In particular, for every $A \neq 0$, there exists exactly one trajectory on $W_c(A,0,0)$, which approaches the equilibrium point $(A,0,0)$ as $\tau \to -\infty$ if $\pm A > 0$ and $\tau \to +\infty$ if $\pm A < 0$.

Proof. Existence of a two-dimensional center manifold $W_c(A,0,0)$, which is tangent to that of the linearized system

$$E_c(A,0,0) = \left\{ w = 0, \quad (\xi, u) \in \mathbb{R}^2 \right\},$$

follows from [4, Theorem 4.1]. We develop an approximation of $W_c(A,0,0)$ by writing

$$w = u^{m+n}\eta(\xi, u), \tag{2.8}$$

where $u^{m+n}\eta(\xi,u)$ is C^1 at the point $(\xi,u) = (A,0)$ with zero partial derivatives. Dynamics along $W_c(A,0,0)$ is given by the two-dimensional system

$$\begin{cases} \dot{\xi} = u^m, \\ \dot{u} = u^{m+n}\eta(\xi, u). \end{cases} \tag{2.9}$$

The function η is to be found by substituting (2.8) into the three-dimensional system (2.4) and using the two-dimensional system (2.9). On doing so, we obtain the following PDE

$$1 \mp \frac{m+1-n}{2(1-n)} A\eta = \mp \frac{1}{1-n} u^{1-n} \pm \frac{m+1-n}{2(1-n)}(\xi - A)\eta + \eta \frac{\partial}{\partial u}(u^{m+n}\eta) + u^m \frac{\partial \eta}{\partial \xi}. \tag{2.10}$$

If $m > 0$, $n < 1$, $m + n > 1$, and $u^{m+n}\eta(\xi,u)$ is a C^1 function at $(\xi,u) = (A,0)$ with zero partial derivatives, then (2.10) has a solution, which is represented asymptotically by (2.6). This computation yields the center manifold $W_c(A,0,0)$ in the form (2.5). Substituting (2.6) into (2.9) and truncating the remainder term, we obtain the truncated normal form (2.7).

From the second equation of the system (2.7), it follows that if $\pm A > 0$, then $\dot{u} > 0$ such that $u(\tau) \to 0$ as $\tau \to -\infty$, whereas if $\pm A < 0$, then $\dot{u} < 0$ such that $u(\tau) \to 0$ as $\tau \to +\infty$. From the first equation of the system (2.7), the constant of integration for ξ is arbitrary, so that $\xi(\tau) \to \tilde{A}$ in the same limit with some $\tilde{A}$. Hence, dynamics along the two-dimensional manifold $W_c(A,0,0)$ is decomposed between a curve of equilibrium states with $u = 0$ and weakly unstable (if $\pm A > 0$) or weakly stable (if $\pm A < 0$) evolution along a curve parameterized by small positive u.

Persistence of the dynamics on $W_c(A,0,0)$ with respect to the remainder terms in (2.6) follows from analysis of the system (2.9). ∎

Proposition 2.2. *For every $m > 1$, $n < 1$, and $m + n > 1$ and for every $\pm A < 0$, there exists a one-dimensional unstable manifold of the dynamical system (2.4) near the equilibrium point $(A,0,0)$, which can be parameterized as follows:*

$$W_u(A,0,0) = \left\{ \xi = A + \mathcal{O}(u^m), \quad w = \mp \frac{m+1-n}{2(1-n)} Au + \mathcal{O}(u^{m+n}), \quad u \in (0,\delta) \right\}, \tag{2.11}$$

where $\delta > 0$ is small. Dynamics of the system (2.4) on the unstable manifold $W_u(A,0,0)$ is topologically equivalent to dynamics of the linear equation

$$\dot{u} = \mp\frac{m+1-n}{2(1-n)}Au. \tag{2.12}$$

Proof. Existence of a one-dimensional unstable manifold $W_u(A,0,0)$, which is tangent to that of the linearized system

$$E_u(A,0,0) = \left\{\xi = A, \quad w = \mp\frac{m+1-n}{2(1-n)}Au, \quad u \in \mathbb{R}\right\},$$

follows from [4, Theorem 4.1]. We develop an approximation of $W_u(A,0,0)$ by writing

$$\begin{cases} \xi = A + u^m\phi(u), \\ w = \mp\frac{m+1-n}{2(1-n)}Au + u^{m+n}\theta(u), \end{cases} \tag{2.13}$$

where $u^m\phi(u)$ and $u^{m+n}\theta(u)$ are C^1 with the zero derivative at $u = 0$. Dynamics along $W_u(A,0,0)$ are given by the one-dimensional system

$$\dot{u} = \mp\frac{m+1-n}{2(1-n)}Au + u^{m+n}\theta(u). \tag{2.14}$$

The functions ϕ and θ are to be found by substituting (2.13) into the three-dimensional system (2.4) and using the one-dimensional system (2.14). By doing so, we obtain the following system of differential equations

$$\left(m\phi(u) + u\frac{d\phi}{du}\right)\left(\mp\frac{m+1-n}{2(1-n)}A + u^{m+n-1}\theta(u)\right) = 1 \tag{2.15}$$

and

$$\begin{aligned} &\left((m+n)\theta(u) + u\frac{d\theta}{du}\right)\left(\mp\frac{m+1-n}{2(1-n)}A + u^{m+n-1}\theta(u)\right) \\ &\quad = 1 \pm \frac{1}{1-n}u^{1-n} + \frac{m+1-n}{2(1-n)}\phi(u)\left(\frac{m+1-n}{2(1-n)}Au^{1-n} \mp u^m\theta(u)\right). \end{aligned} \tag{2.16}$$

If $m > 1$, $n < 1$, and $m + n > 1$, while $u^m\phi(u)$ and $u^{m+n}\theta(u)$ are C^1 with the zero derivative at $u = 0$, then system (2.15) and (2.16) has a solution such that

$$\phi(u) = \mp\frac{2(1-n)}{m(m+1-n)A} + \mathcal{O}(u^{m+n-1}) \tag{2.17}$$

and

$$\theta(u) = \mp\frac{2(1-n)}{(m+n)(m+1-n)A} + \mathcal{O}(u^{\min\{m,1-n,m+n-1\}}). \tag{2.18}$$

The representation (2.13) with (2.17) and (2.18) is equivalent to (2.11). Substituting (2.17) for $\theta(u)$ into (2.14) and truncating the remainder terms, we obtain the linear equation (2.12). Persistence of the linear dynamics on $W_u(A,0,0)$ with respect to the remainder terms in $\theta(u)$ follows from analysis of the differential equation (2.14). ∎

Remark 1. For every $m > 1$, $n < 1$, $m + n > 1$ and for every $\pm A > 0$, one can construct a one-dimensional stable manifold $W_s(A,0,0)$ of the dynamical system (2.4) near the equilibrium

point $(A,0,0)$, which exists for $\xi > A$, $u > 0$, and $w < 0$. However, this stable manifold does not contain trajectories that approach the equilibrium point $(A,0,0)$ as $\tau \to -\infty$.

Remark 2. If $m \in (0,1)$, the function $u^m\phi(u)$ in the proof of Proposition 2.2 is no longer C^1 at $u = 0$. However, the expansions (2.17) and (2.18) are well defined for every $m > 0$, $n < 1$, and $m + n > 1$. Therefore, the result of Proposition 2.2 can be extended for $m \in (0,1)$ and $m = 1$.

Proof of Theorem 1.1. For every $m > 0$, $n < 1$, $m + n > 1$ and for every $\pm A \neq 0$, Proposition 2.1 states that the equilibrium state $(A,0,0)$ is connected by the trajectories of the dynamical system (2.4) with $u(\tau) > 0$ as $\tau \to -\infty$ if and only if $\pm A > 0$. In this case, there exists exactly one trajectory with $u > 0$ such that $u(\tau) \to 0$ as $\tau \to -\infty$. This trajectory belongs to the center manifold $W_c(A,0,0)$, whose dynamics satisfy the system (2.9). From this system, we obtain a first-order nonautonomous equation

$$\frac{du}{d\xi} = u^n \eta(\xi,u) = \pm \frac{2(1-n)}{(m+1-n)A} u^n \left[1 + \mathcal{O}(\xi - A, u^{\min\{1-n,m+n-1\}})\right], \tag{2.19}$$

where the approximation is defined in the limit of $\xi \to A$ and $u \to 0$. Integrating (2.19) near $\xi = A$, we recover the asymptotic behavior (1.14).

For every $m > 0$, $n < 1$, $m + n > 1$ and for every $\pm A < 0$, Proposition 2.2 and Remark 2 state that the equilibrium state $(A,0,0)$ is connected by exactly one trajectory of the dynamical system (2.4) with $u > 0$ and $u(\tau) \to 0$ as $\tau \to -\infty$. This trajectory belongs to the unstable manifold $W_u(A,0,0)$ with the dynamics satisfying (2.14). From (2.13) and (2.17), we obtain

$$\xi = A + u^m \left[\mp \frac{2(1-n)}{m(m+1-n)A} + \mathcal{O}(u^{m+n-1}) \right] \quad \text{as} \quad u \to 0. \tag{2.20}$$

Inverting this nonlinear equation near $\xi = A$, we recover the asymptotic behavior (1.15). ∎

3. Invariant manifolds for large values of $H_\pm$. The trajectories departing from the equilibrium point $(A,0,0)$ of the dynamical system (2.4) are expected to arrive at infinite values for ξ and u. In order to study the behavior of trajectories near infinite values for ξ and u, we shall define $y = 1/u$, which maps an infinite value for u to a zero value for y. The other variables ξ and w must be adjusted accordingly for small values of y. Let us consider the following scaling transformation,

$$\xi = \frac{x}{y^p}, \quad u = \frac{1}{y}, \quad w = \frac{z}{y^q}, \tag{3.1}$$

where (x,y,z) is the set of new variables, and the positive parameters p and q are to be chosen below. Substituting the transformation (3.1) into the dynamical system (2.4), we obtain the following autonomous system in $\mathbb{R}^3$:

$$\begin{cases} \dot{x} = y^{p-m} - pxzy^{1-q}, \\ \dot{y} = -zy^{2-q}, \\ \dot{z} = \pm \frac{1}{1-n} y^{q-m-1} + y^{q-m-n} \mp \frac{m+1-n}{2(1-n)} xzy^{-p} - qz^2 y^{1-q}, \end{cases} \tag{3.2}$$

where a dot still denotes a derivative with respect to the time variable τ.

The system (3.2) is singular at $y = 0$, no matter what positive values of p and q are chosen. To unfold the singularity, we can now introduce a convenient parameterization of solutions with the time variable s instead of the variable τ such that

$$\frac{d\tau}{ds} = y^p, \quad y \geq 0.$$

The map $s \mapsto \tau$ is increasing and we can consider solutions parameterized by the new time variable s such that $y \to 0$ as $s \to +\infty$ (which could correspond to a finite value for the old time variable τ).

With the parameterization $s \mapsto \tau$, the system (3.2) can be rewritten in the equivalent form

$$\left\{ \begin{array}{l} x' = y^{2p-m} - pxzy^{p+1-q}, \\ y' = -zy^{p+2-q}, \\ z' = \pm\frac{1}{1-n} y^{p+q-m-1} + y^{p+q-m-n} \mp \frac{m+1-n}{2(1-n)} xz - qz^2 y^{p+1-q}, \end{array} \right. \tag{3.3}$$

where a prime denotes a derivative with respect to the new time variable s. With the choice $p + 1 = q$, the system (3.3) is rewritten as

$$\left\{ \begin{array}{l} x' = y^{2p-m} - pxz, \\ y' = -zy, \\ z' = \pm\frac{1}{1-n} y^{2p-m} + y^{2p-m+1-n} \mp \frac{m+1-n}{2(1-n)} xz - qz^2. \end{array} \right. \tag{3.4}$$

The power singularity is unfolded if we choose $2p - m = 1 - n$ and replace y^{1-n} with another variable. Thus, a suitable choice of parameters p and q is given by

$$\left\{ \begin{array}{l} p + 1 = q, \\ 2p - m = 1 - n, \end{array} \right. \quad \Rightarrow \quad \left\{ \begin{array}{l} p = \frac{m+1-n}{2}, \\ q = \frac{m+3-n}{2}. \end{array} \right. \tag{3.5}$$

Denoting y^{1-n} by $\tilde{y}$ and dropping the tilde notation, we finally obtain the explicit form of the transformations (3.1),

$$\xi = \frac{x}{y^{\frac{m+1-n}{2(1-n)}}}, \quad u = \frac{1}{y^{\frac{1}{1-n}}}, \quad w = \frac{z}{y^{\frac{m+3-n}{2(1-n)}}}. \tag{3.6}$$

With the transformation (3.6), the system (3.4) is rewritten in the simplest nonsingular form with a quadratic vector field:

$$\left\{ \begin{array}{l} x' = y - \frac{m+1-n}{2} xz, \\ y' = -(1-n)zy, \\ z' = \pm\frac{1}{1-n} y + y^2 \mp \frac{m+1-n}{2(1-n)} xz - \frac{m+3-n}{2} z^2, \end{array} \right. \tag{3.7}$$

where we recall that $m > 0$, $n < 1$, and $m + n > 1$.

The family of equilibrium points for the system (3.7) is given by $(x, y, z) = (x_0, 0, 0)$, where $x_0 \in \mathbb{R}$ is an arbitrary parameter. Each equilibrium point is associated with the Jacobian matrix

$$\left[\begin{array}{ccc} 0 & 1 & -\frac{m+1-n}{2} x_0 \\ 0 & 0 & 0 \\ 0 & \pm\frac{1}{1-n} & \mp\frac{m+1-n}{2(1-n)} x_0 \end{array} \right].$$

This Jacobian matrix has a double zero eigenvalue (with two linearly independent eigenvectors) and a simple eigenvalue $\mp x_0(m+1-n)/(2-2n)$.

In the context of reversing and antireversing interfaces, we are interested in the behavior of solutions for which $\xi \to +\infty$ and $u \to +\infty$. It follows from the transformation (3.6), that this requirement restricts our consideration to the family of critical points $(x_0, 0, 0)$ with $x_0 > 0$. If $x_0 > 0$, the linearization of the dynamical system (3.7) at the equilibrium point $(x_0, 0, 0)$ has a two-dimensional center manifold and a one-dimensional stable (upper sign) or unstable (lower sign) manifold. Since the vector field of the dynamical system (3.7) is analytic (quadratic), another straightforward application of the invariant manifold theorems [12, 18] yields that the equilibrium point $(x_0, 0, 0)$ with $x_0 > 0$ is located at the intersection of the two invariant manifolds, which are tangential to the invariant manifolds of the linearized system. We formulate these results in the following Propositions 3.1 and 3.2. The relevant conclusions on the behavior of solutions of the differential equations (1.8) for large values of $H_\pm$ expressed in Theorem 1.2 follow from these two propositions.

Proposition 3.1. *Assume $m > 0$, $n < 1$, and $m + n > 1$. For every $x_0 > 0$, there exists a two-dimensional center manifold of the dynamical system (3.7) near the equilibrium point $(x_0, 0, 0)$, which can be parameterized as follows:*

$$W_c(x_0,0,0) = \left\{ y = \frac{m+1-n}{2} xz + z^2 g(x,z), \quad x \in (x_0-\delta, x_0+\delta), \quad z \in (-\delta,\delta) \right\}, \tag{3.8}$$

where

$$g(x,z) = \pm(1-n)\left(\frac{m+n+1}{2} - \frac{(m+1-n)^2}{4} x_0^2 \right) + \mathcal{O}(x-x_0, z) \tag{3.9}$$

and $\delta > 0$ is small. The dynamics of the system (3.7) on the center manifold $W_c(x_0, 0, 0)$ is topologically equivalent to the dynamics at the truncated normal form

$$\begin{cases} x' = \pm(1-n)\left(\frac{m+n+1}{2} - \frac{(m+1-n)^2}{4} x_0^2 \right) z^2, \\ z' = -(1-n) z^2. \end{cases} \tag{3.10}$$

In particular, there exists exactly one trajectory on $W_c(x_0, 0, 0)$, which approaches the equilibrium point $(x_0, 0, 0)$ as $s \to +\infty$.

Proof. Existence of a two-dimensional center manifold $W_c(x_0, 0, 0)$, which is tangent to that of the linearized system

$$E_c(x_0,0,0) = \left\{ y = \frac{m+1-n}{2} x_0 z, \quad (x,z) \in \mathbb{R}^2 \right\},$$

follows from [4, Theorem 4.1]. We develop an approximation of $W_c(x_0, 0, 0)$ by writing $y = f(x, z)$ and expanding f using a Taylor series in small values of both $x - x_0$ and z. Dynamics along $W_c(x_0, 0, 0)$ is given by the two-dimensional system

$$\begin{cases} x' = f(x,z) - \frac{m+1-n}{2} xz, \\ z' = \pm \frac{1}{1-n} f(x,z) + f(x,z)^2 \mp \frac{m+1-n}{2(1-n)} xz - \frac{m+3-n}{2} z^2. \end{cases} \tag{3.11}$$

The function f is to be found from the PDE

$$\frac{\partial f}{\partial x}\left[f - \frac{m+1-n}{2}xz\right] + \frac{\partial f}{\partial z}\left[\pm\frac{1}{1-n}f + f^2 \mp \frac{m+1-n}{2(1-n)}xz - \frac{m+3-n}{2}z^2\right] + (1-n)zf = 0. \tag{3.12}$$

Equations (3.11) and (3.12) suggest the following near-identity transformation of the function f given by

$$f(x,z) = \frac{m+1-n}{2}xz + z^2 g(x,z). \tag{3.13}$$

After the near-identity transformation (3.13), the dynamics along $W_c(x_0,0,0)$ are given by the two-dimensional system

$$\begin{cases} x' = z^2 g(x,z), \\ z' = z^2\left[\pm\frac{1}{1-n}g(x,z) - \frac{m+3-n}{2} + \left(\frac{m+1-n}{2}x + zg(x,z)\right)^2\right]. \end{cases} \tag{3.14}$$

The function g is now to be found from the PDE

$$\frac{m+1-n}{2}(1-n)x + zg\left(\frac{m+3-3n}{2} + z\frac{\partial g}{\partial x}\right) + \left(\frac{m+1-n}{2}x + 2zg + z^2\frac{\partial g}{\partial z}\right)\left(\pm\frac{1}{1-n}g + \left(\frac{m+1-n}{2}x + zg\right)^2 - \frac{m+3-n}{2}\right) = 0,$$

which has a solution satisfying the asymptotic expansion (3.9). Representation (3.13) yields (3.8). Substituting (3.9) into (3.14) and truncating at the cubic terms, we obtain the truncated normal form (3.10).

From the second equation of the system (3.10), it follows that there exists a unique solution such that $z(s) \to 0$ as $s \to +\infty$ with $z > 0$. From the first equation of the system (3.10), the constant of integration for x is arbitrary, so that $x(s) \to \tilde{x}_0$ as $s \to +\infty$ with some $\tilde{x}_0$. Hence, dynamics along the two-dimensional manifold $W_c(x_0,0,0)$ is decomposed between a curve of equilibrium states with $z = 0$ and weakly stable evolution along a curve parameterized by small positive z. Persistence of the dynamics on $W_c(x_0,0,0)$ with respect to the remainder terms in (3.9) follows from analysis of the system (3.14). ∎

Proposition 3.2. *Assume $m > 0$, $n < 1$, and $m + n > 1$. For every $x_0 > 0$, there exists a one-dimensional stable (upper sign) or unstable (lower sign) manifold of the dynamical system (3.7) near the equilibrium point $(x_0,0,0)$, which can be expressed explicitly:*

$$W_{s/u}(x_0,0,0) = \left\{ y = 0, \quad z = \mp\frac{m+1-n}{2(1-n)}x\left[1 - \left(\frac{x}{x_0}\right)^{\frac{2}{m+1-n}}\right], \quad x \in (x_0-\delta, x_0+\delta)\right\}, \tag{3.15}$$

where $\delta > 0$ is small. The dynamics of the system (3.7) on the manifold $W_{s/u}(x_0,0,0)$ is topologically equivalent to the dynamics of the linear equation

$$x' = \mp\frac{m+1-n}{2(1-n)}x_0(x - x_0). \tag{3.16}$$

Proof. The linearized system has the stable/unstable manifold

$$E_{s/u}(x_0,0,0) = \left\{ y = 0, \quad z = \pm\frac{1}{1-n}(x-x_0), \quad x \in \mathbb{R} \right\}.$$

Existence of a one-dimensional manifold $W_{s/u}(x_0,0,0)$ that is tangent to $E_{s/u}(x_0,0,0)$ follows from [4, Theorem 4.1]. We notice from (3.7) that $y = 0$ is an invariant reduction of the three-dimensional system. Therefore, we can set $y = 0$ and seek a parameterization of $W_{s/u}(x_0,0,0)$ by working with $z = \psi(x)$, where $\psi(x_0) = 0$ and $\psi'(x_0) = \pm\frac{1}{1-n}$. Dynamics along $W_{s/u}(x_0,0,0)$ are given by the one-dimensional system

$$x' = -\frac{m+1-n}{2} x\psi(x). \tag{3.17}$$

From the three-dimensional system (3.7), we obtain a linear differential equation for nonzero ψ:

$$x\frac{d\psi}{dx} = \frac{m+3-n}{m+1-n}\psi(x) \pm \frac{1}{1-n}x. \tag{3.18}$$

This equation completed with the initial condition $\psi(x_0) = 0$ admits a unique solution

$$\psi(x) = \mp\frac{m+1-n}{2(1-n)} x \left[1 - \left(\frac{x}{x_0} \right)^{\frac{2}{m+1-n}} \right]. \tag{3.19}$$

Note that $\psi'(x_0) = \pm 1/(1-n)$, because $W_{s/u}(x_0,0,0)$ is tangent to $E_{s/u}(x_0,0,0)$. Substituting

$$\psi(x) = \pm\frac{1}{1-n}(x-x_0) + \mathcal{O}((x-x_0)^2) \tag{3.20}$$

into the differential equation (3.17) and truncating at the quadratic remainder term, we obtain the linear equation (3.16). Persistence of the linear dynamics on $W_{s/u}(x_0,0,0)$ with respect to the remainder term follows from analysis of the system (3.17) with the expansion (3.20). ∎

Proof of Theorem 1.2. For every $x_0 > 0$, Proposition 3.1 states that there exists exactly one trajectory with $y > 0$ such that $y(s) \to 0$ as $s \to +\infty$. This trajectory belongs to the center manifold $W_c(x_0,0,0)$, whose dynamics satisfy the system (3.11). We recover the asymptotic behavior (1.16) by eliminating y from the transformation (3.6) and setting $x = x_0$.

For every $x_0 > 0$, Proposition 3.2 states that the point $(x_0,0,0)$ is an intersection of the two-dimensional center manifold $W_c(x_0,0,0)$ and the one-dimensional stable/unstable manifold $W_{s/u}(x_0,0,0)$ for the upper/lower sign. Therefore, the point can be reached in the direction $s \to +\infty$ along $W_s(x_0,0,0)$ but cannot be reached along $W_u(x_0,0,0)$. This guarantees that the trajectory in Proposition 3.1 with $y > 0$ such that $y(s) \to 0$ as $s \to +\infty$ is unique for the lower sign. Therefore, for every $x_0 > 0$, there exists a one-dimensional set of solutions of the differential equation (1.8) for the lower sign such that $H_-(\xi) \to +\infty$ as $\xi \to +\infty$.

On the other hand, the span of the trajectory in Proposition 3.1 and the trajectory in Proposition 3.2 is a two-dimensional set that hosts all trajectories with $y > 0$ such that

$y(s) \to 0$ as $s \to +\infty$. Therefore, for every $x_0 > 0$, there exists a two-dimensional set of solutions of the differential equation (1.8) for the upper sign such that $H_+(\xi) \to +\infty$ as $\xi \to +\infty$. The rate of change along $W_s(x_0, 0, 0)$ is exponential in s and the rate of change along $W_c(x_0, 0, 0)$ is algebraic in s. Therefore, solutions along the two-dimensional set still obey the asymptotic behavior (1.16). ∎

4. Connection of invariant manifolds. Let us summarize the results of the previous two sections on the existence of solutions $H_\pm$ to the differential equations (1.8) on the semi-infinite line $(A_\pm, \infty)$ that satisfy the properties (1.9)–(1.11). Such solutions are related to the trajectories of the dynamical systems (2.4) and (3.7), which depart from the equilibrium points where $H_\pm$ is zero and arrive at the equilibrium point where $H_\pm$ is infinite. In what follows, we will consider separately the two different systems for H_+ and H_-.

4.1. The system for $H_+(t > 0)$. By Propositions 2.1 and 2.2, for every nonzero $A \equiv A_+$, there is a unique trajectory of the dynamical system (2.4) in variables (ξ, u, w) that departs from the equilibrium point $(A_+, 0, 0)$ as $\tau \to -\infty$ and belongs to the domain $u > 0$. This trajectory is contained in the center manifold $W_c(A_+, 0, 0)$ if $A_+ > 0$ and in the unstable manifold $W_u(A_+, 0, 0)$ if $A_+ < 0$.

By Propositions 3.1 and 3.2, for every $x_0 > 0$, there is a two-dimensional set of trajectories of the dynamical system (3.7) in variables (x, y, z) that reaches the equilibrium point $(x_0, 0, 0)$ as $s \to +\infty$ and belongs to the domain $y > 0$.

We shall now establish that the same trajectory departing from the equilibrium point $(A_+, 0, 0)$ in (2.4) arrives at the equilibrium point $(x_0, 0, 0)$ in (3.7). This trajectory determines a unique solution H_+ of the differential equation (1.8) with the upper sign satisfying properties (1.9)–(1.11).

Lemma 4.1. *Fix $A_+ \in \mathbb{R}\backslash\{0\}$ and consider a one-parameter trajectory of the dynamical system (2.4) for the upper sign such that $(\xi, u, w) \to (A_+, 0, 0)$ as $\tau \to -\infty$ and $u > 0$. Then, there exists a $\tau_0 \in \mathbb{R}$ (or $\tau_0 = +\infty$) such that $\xi(\tau) \to +\infty$ and $u(\tau) \to +\infty$ as $\tau \to \tau_0$.*

Proof. We introduce the energy-like quantity for the dynamical system (2.4) with the upper sign:

$$E(w, u) := \frac{1}{2}w^2 - \frac{1}{m+n+1}u^{m+n+1} - \frac{1}{(m+2)(1-n)}u^{m+2}. \tag{4.1}$$

Computing the derivative of E in τ along a solution of system (2.4), we obtain

$$\frac{dE}{d\tau} = -\frac{m+1-n}{2(1-n)}\xi w^2. \tag{4.2}$$

If $A_+ > 0$, then $\xi(\tau) \geq A_+ > 0$, and E is a strictly decreasing function of τ as long as the solution to system (2.4) exists and $w(\tau) \neq 0$. By the representation (2.5) of $W_c(A_+, 0, 0)$ in Proposition 2.1, we have $w(\tau) > 0$ for sufficiently large negative τ. Now $w(\tau)$ cannot vanish for any τ because

$$\text{if } w = 0, \text{ then } \dot{w} = u^{m+n} + \frac{1}{1-n}u^{m+1} > 0, \tag{4.3}$$

which contradicts the positivity of w before vanishing. Therefore, w is bounded away from zero and $E(w,u)$ decreases to $-\infty$ in finite or infinite time τ. Because $E(0,u) \leq E(w,u)$, we have $u \to +\infty$ if $E(w,u) \to -\infty$.

If $A_+ < 0$, then E is an increasing function of τ at least for sufficiently large negative τ. By the representation (2.11) of $W_u(A_+,0,0)$ in Proposition 2.2, we still have $w(\tau) > 0$ for sufficiently large negative τ. Also, $w(\tau)$ cannot vanish for any τ by the same contradiction, since (4.3) holds. Therefore, $\xi(\tau)$ and $u(\tau)$ are still increasing functions, and there is a finite $\tau_1 \in \mathbb{R}$ such that $\xi(\tau_1) = 0$ and $\dot{\xi}(\tau_1) > 0$. For $\tau > \tau_1$, E becomes a strictly decreasing function and the energy method described above proves again that $u(\tau) \to +\infty$ in finite or infinite time τ.

We shall now prove that $\xi(\tau) \to +\infty$ as $\tau \to \tau_0$, where τ_0 is either finite or infinite. Since $w > 0$ for all $\tau \in (-\infty, \tau_0)$, the map $\tau \to u$ is monotonically increasing, so that we can parameterize both ξ and w by u and consider the limit $u \to +\infty$. From the last two equations of the system (2.4), we obtain

$$w\frac{dw}{du} = u^{m+n} + \frac{1}{1-n}u^{m+1} - \frac{m+1-n}{2(1-n)}\xi w. \tag{4.4}$$

Since $\xi(\tau) > 0$ for τ close to τ_0 and $w(\tau) > 0$ for all $\tau \in (-\infty, \tau_0)$, we estimate for τ close to τ_0,

$$\frac{d}{du}\left(\frac{1}{2}w^2\right) \leq u^{m+n} + \frac{1}{1-n}u^{m+1}.$$

Integrating this differential inequality, we obtain

$$w^2 \leq C + \frac{2}{m+n+1}u^{m+n+1} + \frac{2}{(m+2)(1-n)}u^{m+2}, \tag{4.5}$$

where $C > 0$ is a constant of integration. Therefore, as $u \to \infty$, there exists a constant $w_\infty > 0$ such that $w \leq w_\infty u^{(m+2)/2}$ for sufficiently large u. From the first two equations of the system (2.4), we obtain

$$\frac{d\xi}{du} = \frac{u^m}{w} \geq \frac{u^{\frac{m-2}{2}}}{w_\infty}. \tag{4.6}$$

Integrating this differential inequality, we obtain a lower bound for ξ given by

$$\xi \geq C + \frac{2}{mw_\infty}u^{\frac{m}{2}}, \tag{4.7}$$

where $C > 0$ is another constant of integration. This lower bound yields $\xi \to +\infty$ as $u \to +\infty$. ∎

Corollary 4.2. *The trajectory of Lemma 4.1 such that $\xi(\tau) \to +\infty$ and $u(\tau) \to +\infty$ corresponds to the trajectory of system (3.7) approaching the equilibrium state $(x_0, 0, 0)$ for some $x_0 \in [0, \infty)$. Consequently, one can define a piecewise C^1 map*

$$\mathbb{R}\backslash\{0\} \ni A_+ \mapsto x_0 \in \mathbb{R}^+. \tag{4.8}$$

Proof. We can use the transformation (3.6). Since $u \to \infty$, then $y \to 0$. From the bound (4.5), we obtain

$$z = wu^{-\frac{m+3-n}{2}} \leq w_\infty u^{-\frac{1-n}{2}}. \tag{4.9}$$

Therefore, $z \to 0$ as $u \to \infty$. On the other hand, from the bound (4.7), we only obtain

$$x = \xi u^{-\frac{m+1-n}{2}} \geq C u^{-\frac{1-n}{2}},$$

which is not sufficient to claim that x remains bounded as $u \to \infty$.

Using (3.6), (4.4), and (4.6), we obtain the following system for x and z in the variable u:

$$\frac{dx}{du} = \frac{1}{u}\left[\frac{1}{zu^{1-n}} - \frac{m+1-n}{2}x\right] \tag{4.10}$$

and

$$\frac{dz}{du} = \frac{1}{1-n}\frac{dx}{du} + \frac{1}{u}\left[\frac{1}{zu^{2-2n}} - \frac{m+3-n}{2}z\right]. \tag{4.11}$$

It follows from the bound (4.9) and (4.11) that there is a positive constant C such that

$$\frac{d}{du}\left(z - \frac{1}{1-n}x\right) \geq -Cu^{-\frac{3-n}{2}}$$

for sufficiently large u. Since $u^{-(3-n)/2}$ is integrable as $u \to +\infty$, then $z - x/(1-n)$ is bounded from below by a negative constant. Since z is bounded and approaches zero as $u \to \infty$, we obtain that x is bounded from above by a positive constant for all sufficiently large u. Finally, $(x_0, 0, 0)$ is an equilibrium state of system (3.7); therefore, the trajectory approaches $(x_0, 0, 0)$ for some $x_0 \in [0, \infty)$. ∎

Remark 3. Integrating (4.10), we obtain

$$x = \frac{c}{u^{\frac{m+1-n}{2}}} + \frac{1}{u^{\frac{m+1-n}{2}}}\int \frac{u^{\frac{m-1-n}{2}}du}{u^{1-n}z},$$

where c is an arbitrary constant. If we can prove that $\lim_{u\to\infty} u^{1-n}z(u) = a_\infty > 0$, then

$$\lim_{u\to\infty} x(u) = \frac{2}{a_\infty(m+1-n)} \in (0, \infty).$$

This would indicate that the bound (4.9) is not sharp. However, we only have numerical data supporting this claim for every $A_+ \in \mathbb{R}$.

We will show numerically in section 5 for $n = 0$ that both pieces of the map (4.8) are monotonically increasing for all $A_+ \in \mathbb{R}$ and intersecting at $x = x_Q$ for $A_+ = 0$, where

$$x_Q := \frac{\sqrt{2(m+n+1)}}{m+1-n}. \tag{4.12}$$

The exact value x_Q corresponds to the exact solution (1.17) of the scalar differential equations (1.8). This exact solution is recovered with the following elementary result.

Proposition 4.3. *There exists an exact solution of the dynamical system (3.7) given by*

$$\begin{cases} x(s) = x_Q, \\ y(s) = \frac{b\sqrt{m+n+1}}{\sqrt{2}(1+(1-n)bs)}, \\ z(s) = \frac{b}{1+(1-n)bs}, \end{cases} \qquad s > -\frac{1}{b(1-n)}, \tag{4.13}$$

where x_Q is given by (4.12) and b is an arbitrary positive parameter.

Proof. Consider the system (3.7) and try the reduction $x = x_0$, where x_0 is constant in s. Then, on setting $y = \frac{m+1-n}{2} x_0 z$ we obtain the following differential equations:

$$y' = -(1-n)zy, \quad z' = y^2 - \frac{m+3-n}{2} z^2.$$

This system is compatible with the constraint on y if $z' = -(1-n)z^2$ and $x_0^2 = x_Q^2$. The general solution of $z' = -(1-n)z^2$ is

$$z(s) = \frac{b}{1+(1-n)bs}$$

for a positive parameter b. The solution is defined for $s > -1/(b(1-n))$. ∎

Remark 4. It follows from (3.6) and (4.13) that $\xi \to 0$ and $u \to 0$ as $s \to -1/(b(1-n))$. Therefore, the exact solution of Proposition 4.3 corresponds to the choice $A_+ = 0$ in Lemma 4.1.

4.2. The system for $H_-(t < 0)$. By Propositions 2.1 and 2.2, for every nonzero $A \equiv A_-$, there is a unique trajectory of the dynamical system (2.4) in variables (ξ, u, w) that departs from the equilibrium point $(A_-, 0, 0)$ as $\tau \to -\infty$ and belongs to the domain $u > 0$. This trajectory is contained in the unstable manifold $W_u(A_-, 0, 0)$ if $A_- > 0$ and in the center manifold $W_c(A_-, 0, 0)$ if $A_- < 0$.

By Propositions 3.1 and 3.2, for every $x_0 > 0$, there is a unique trajectory of the dynamical system (3.7) in variables (x, y, z) that reach the equilibrium point $(x_0, 0, 0)$ as $s \to +\infty$ and belongs to the domain $y > 0$. This trajectory is contained in the center manifold $W_c(x_0, 0, 0)$.

If we try an argument used in the proof of Lemma 4.1, then it becomes clear that most of the trajectories departing from the equilibrium point $(A_-, 0, 0)$ in system (2.4) will not arrive at the equilibrium point $(x_0, 0, 0)$ in system (3.7) but instead reach the value $u = 0$ in a finite $\tau \in \mathbb{R}$. This indicates that, first, there are very few values of A_-, for which the trajectories may reach infinite values for u and, second, the numerical method should not be based on the trajectories departing from the equilibrium point $(A_-, 0, 0)$ (such a shooting method was used previously in [6]). Instead, it may be better to look for the unique trajectory departing the equilibrium point $(x_0, 0, 0)$ in system (3.7) in the negative direction of the time variable s.

To illustrate the previous point, we show on Figure 1 the trajectories of the system (2.4) with $m = 3$ and $n = 0$ starting from the equilibrium point $(A_\pm, 0, 0)$ along either center (for $A_+ > 0$) or unstable (for $A_- > 0$) manifolds. The trajectories of the system for H_+ extend from small to infinite values of H_+; see panel (a). In contrast, the trajectories of the system

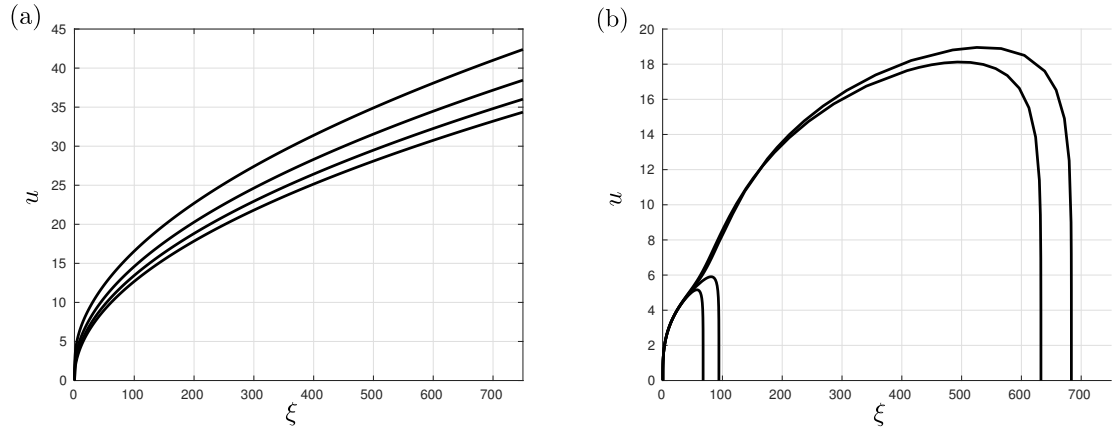

Figure 1. *Panels* (a) *and* (b) *show trajectories of the system* (2.4) *with* $m = 3$ *and* $n = 0$ *for* H_+ *and* H_-, *respectively. In both cases, the trajectories start from the equilibrium point* $(A_\pm, 0, 0)$ *and depart along either the center or the unstable manifolds.*

for H_- turn back and return to small values of H_-; see panel (b). Note that the return time is significantly different between the first two and the last two trajectories. This indicates the presence of a particular value of A_- for which there exists a trajectory that extends from small to infinite values of H_-; see (5.4) below.

In order to justify our numerical scheme, we shall prove that the trajectory departing the equilibrium point $(x_0, 0, 0)$ in system (3.7) in the negative s direction either intersects the plane $u = 0$ or the plane $w = 0$ of system (2.4).

Lemma 4.4. *Fix* $x_0 > 0$ *and consider a one-parameter trajectory of the dynamical system* (3.7) *for the lower sign such that* $(x, y, z) \to (x_0, 0, 0)$ *as* $s \to +\infty$ *and* $y > 0$. *Then, there exists an* $s_0 \in \mathbb{R}$ *(or* $s_0 = -\infty$*) such that*

(i) *either* $z(s_0) = 0$ *and* $y(s_0) \in (0, \infty]$

(ii) *or* $y(s) \to +\infty$ *as* $s \to s_0$, *whereas* $\lim_{s\to s_0} z(s)y(s)^{-\frac{m+3-n}{2(1-n)}} \in [0, \infty)$.

Proof. For convenience, let us reverse the time variable, by transforming $s \to -s$, and rewrite system (3.7) with the lower sign in the negative direction of s:

$$\begin{cases} x' = \frac{m+1-n}{2}xz - y, \\ y' = (1-n)zy, \\ z' = \frac{1}{1-n}y - y^2 - \frac{m+1-n}{2(1-n)}xz + \frac{m+3-n}{2}z^2. \end{cases} \tag{4.14}$$

By Proposition 3.1, we have $y > 0$ and $z > 0$ for the trajectory departing from the equilibrium point $(x_0, 0, 0)$ (in negative s) along $W_c(x_0, 0, 0)$. From the second equation of system (4.14), y remains an increasing function of negative s as long as z remains positive. Therefore, we have an alternative: either z vanishes before y diverges or y diverges before z vanishes.

The first choice of the alternative gives case (i). For the second choice, let us consider variables ξ and w given by (3.6) and parameterized by y in the limit $y \to +\infty$ (the map $s \mapsto y$

is one-to-one and onto). By dividing the first and third equations in system (4.14) by the second equation, we obtain

$$\frac{dx}{dy} = \frac{m+1-n}{2(1-n)}\frac{x}{y} - \frac{1}{(1-n)z}, \quad \frac{dz}{dy} = \frac{1-(1-n)y}{(1-n)^2 z} - \frac{m+1-n}{2(1-n)^2}\frac{x}{y} + \frac{m+3-n}{2(1-n)}\frac{z}{y}.$$

By using variables ξ and w given by (3.6), we obtain

$$\frac{d\xi}{dy} = -\frac{1}{(1-n)y^{\frac{m+2-n}{1-n}}w}, \quad \frac{dw}{dy} = \frac{1-(1-n)y}{(1-n)^2 y^{\frac{m+3-n}{1-n}}w} - \frac{m+1-n}{2(1-n)^2}\frac{\xi}{y^{\frac{2-n}{1-n}}}. \tag{4.15}$$

To show that the second choice of the alternative above gives case (ii), we will prove that w remains finite as $y \to +\infty$. This is done by a contradiction. Assume that $w \to +\infty$ as $y \to +\infty$. Therefore, there exists $w_0 > 0$ such that $w \geq w_0$ for all sufficiently large y. Then, from the first equation of system (4.15), we have for sufficiently large y,

$$\left|\frac{d\xi}{dy}\right| \leq \frac{1}{(1-n)y^{\frac{m+2-n}{1-n}}w_0}.$$

Because $y^{-(m+2-n)/(1-n)}$ is integrable at infinity, there is a finite positive ξ_∞ such that $|\xi| \leq \xi_\infty$ for all sufficiently large y. Then, from the second equation of system (4.15), we obtain for sufficiently large y,

$$\left|\frac{dw}{dy}\right| \leq \frac{1}{(1-n)y^{\frac{m+2}{1-n}}w_0} + \frac{m+1-n}{2(1-n)^2}\frac{\xi_\infty}{y^{\frac{2-n}{1-n}}}.$$

Since both $y^{-(m+2)/(1-n)}$ and $y^{-(2-n)/(1-n)}$ are integrable at infinity, there is a finite positive w_∞ such that $w \leq w_\infty$ for all sufficiently large y, contradicting the assumption that $w \to +\infty$ as $y \to +\infty$. Therefore, case (ii) is proved. ∎

Corollary 4.5. *The trajectory of system (3.7) departing from the equilibrium point $(x_0, 0, 0)$ with $x_0 > 0$ in the negative direction of s intersects either the half-plane $w = 0$ and $u \geq 0$ in system (2.4) in case (i) of Lemma 4.4 or the half-plane $u = 0$, $w \geq 0$ in system (2.4) in case (ii). Moreover, in the corresponding cases,*

(i) *if $\lim_{s\to s_0} u(s) > 0$, then $\lim_{s\to s_0} |\xi(s)| < \infty$;*
(ii) *if $\lim_{s\to s_0} w(s) > 0$, then $\lim_{s\to s_0} |\xi(s)| < \infty$.*

Consequently, one can define two piecewise C^1 maps

$$\text{(i)} \quad \mathbb{R}^+ \ni x_0 \mapsto (\xi, u) \in \mathbb{R} \times \mathbb{R}^+ \quad \text{and} \quad \text{(ii)} \quad \mathbb{R}^+ \ni x_0 \mapsto (\xi, w) \in \mathbb{R} \times \mathbb{R}^+. \tag{4.16}$$

Proof. In case (i), it is trivial to see that $z(s_0) = 0$ and $y(s_0) \in (0, +\infty]$ corresponds to the half-plane $w = 0$ and $u \geq 0$. The first equation of systems (4.14) and (4.15) can be written for the variable ξ as follows:

$$\xi' = -y^{\frac{1-m-n}{2(1-n)}},$$

where the prime still denotes the derivative with respect to the time variable s in the negative direction of s. If y remains finite as $s \to s_0$, then ξ is bounded as $s \to s_0$, since the third equation of system (4.14) implies that s_0 is finite in this case.

In case (ii), it is also trivial to see that $\lim_{s\to s_0} y(s) = +\infty$ and

$$\lim_{s\to s_0} z(s)y(s)^{-(m+3-n)/(2-2n)} \in [0,\infty)$$

corresponds to the half-plane $u = 0$ and $w \geq 0$. If w remains nonzero in the limit $y \to +\infty$, then there exists $w_0 > 0$ such that $w \geq w_0$ for all sufficiently large y. Then, the same analysis as in Lemma 4.4 applies to the first equation of system (4.15) and shows that ξ remains finite as $y \to +\infty$. ∎

Unfortunately, we do not control the value of ξ at the intersection of the two piecewise C^1 maps (4.16). However, we will show numerically in section 5 for $n = 0$ that the piecewise C^1 maps (4.16) are typically connected at the points where $u = w = 0$ and $\xi = A \in \mathbb{R}$. In this case, a true solution H_- of the differential equation (1.8) with the lower sign satisfying properties (1.9)–(1.11) exists.

5. Numerical results for the self-similar solutions. Let us describe a new numerical approach, based on the results of Lemmas 4.1 and 4.4, that will be used to furnish meaningful solutions to the differential equations (1.8), for H_- and H_+. In sections 5.1 and 5.2 we describe the numerical procedures for finding solutions for H_- and H_+, respectively. Finally, in section 5.3, we summarize the results of the numerical experiments and compare them with the results found in Foster et al. [6]. In this section, we set $n = 0$ for all computations.

5.1. Solutions for $H_-(t < 0)$. As discussed in section 4.2, we wish to numerically construct a unique trajectory from infinite to finite values of H_-. To do so, we integrate the system (3.7) from near the equilibrium point $(x_0, 0, 0)$ in the far field towards the equilibrium point $(A_-, 0, 0)$ of the system (2.4) in the near field. The numerical procedure is carried out as follows:

1. Select a value of $x_0 > 0$. Ideally, one would like to begin by using this choice of x_0 to specify unique initial values for $(x, y, z) = (x_0, 0, 0)$, and then numerically integrating the system (3.7) backward in the "time" variable s. Equivalently, one could integrate the system (4.14) forwards in time. However, since $(x_0, 0, 0)$ is an equilibrium point, it is not possible to escape $(x_0, 0, 0)$ in a finite time. Thus, in order to ensure that any numerical integration scheme can depart from near the equilibrium point along the center manifold, $W_c(x_0, 0, 0)$, it is necessary to take a "small step", say $\delta \ll 1$, away from $(x_0, 0, 0)$ using the relevant asymptotic behavior. Using (3.8) and (3.10) with $n = 0$, we find that a trajectory on the center manifold $W_c(x_0, 0, 0)$ has the local behavior

$$\begin{cases} x = x_0 + \left(\frac{m+1}{2} - \left(\frac{m+1}{2}\right)^2 x_0^2\right)\delta + \mathcal{O}(\delta^2), \\ y = \frac{m+1}{2} x_0 \delta + \mathcal{O}(\delta^2), \\ z = \delta \end{cases} \tag{5.1}$$

for small positive values of δ. Having selected values for both x_0 and δ, the behaviors (5.1) may be used to specify unique (pseudo)initial values for (x, y, z) and to begin the numerical integration of the system (3.7) in the direction of decreasing s. In this study, numerical integration of the system (3.7) was carried out using the `ode45` routine in MATLAB with the default settings, except `AbsTol` and `RelTol` which were both set to have a value of 10^{-10}. Selecting an appropriate value of δ is a somewhat ad-hoc procedure: there is trade-off between taking δ too small, which renders it difficult for the numerical integration to escape the

neighborhood of the equilibrium point (leading to poor accuracy of the integration), and taking δ too large which could result in low accuracy of the asymptotic expansion (5.1). However, we found that choosing $\delta \in (10^{-3}, 10^{-2})$ gave good results over the ranges of parameters we studied. Robustness of the results with respect to changes in (i) the choice of δ and (ii) the number of terms in the asymptotic expansion (5.1) were verified.

2. The result of Corollary 4.5 asserts that all such trajectories will ultimately—in either a finite or infinite time—intersect with either the plane $w = 0$ or $u = 0$; see the maps (4.16). To ensure accurate numerical integration of the system in the near field, in variables (ξ, u, w), it is necessary to "switch" from integrating the far-field system (3.7) to the near-field system (2.4) backward in time. The choice of conditions under which this switch should occur is, again, somewhat arbitrary. However, as long as the values of (x, y, z)—and hence the values of (ξ, u, w)—are all finite and nonzero, this switching is valid at any point. In this study, we chose to switch from integrating (3.7) to (2.4) with $n = 0$ when $xy^{-(m+1)/2} = 20$ (or equivalently when $\xi = 20$). However, we verified that our results were robust to changes in the choice of switching conditions. This switching procedure can be readily automated within MATLAB using the `Events` function to autonomously (i) stop the integration of the system (3.7) when the specified conditions are satisfied; (ii) read off the final values of (x, y, z); (iii) transform these to corresponding values for (ξ, u, w) using the change of variables (3.6); (iv) and begin the integration of (2.4) backwards in time from the appropriate initial data.

3. The integration of the system (2.4) is then continued backward in the time variable τ until either $w = 0$ or $u = 0$. Again, we used the `Events` function to autonomously detect when either of these events occurred and to stop the integration. It is noteworthy that we found it helpful to use `ode15s` to integrate the near-field system—again, the default settings were used with the exception of `AbsTol` and `RelTol` which were both set to 10^{-10}. Although `ode15s` is typically slower than `ode45`, it is considerably more appropriate to deal with integrating systems of equations that exhibit apparent stiffness. This apparent stiffness, manifested as rapid changes in the direction of the trajectory in variables (ξ, u, w), arises as an artifact of the infinite time required to reach the equilibrium point $(A_-, 0, 0)$. Thus, if a trajectory approaches very close to the equilibrium point it appears to be rapidly rejected from that neighborhood. When the integration is terminated, we record the following pieces of data: (i) the selected value of x_0; (ii) whether the trajectory reached $u = 0$ or $w = 0$; (iii) and the value of either (ξ, u) or (ξ, w) at the termination point. These data define a point on one of the two piecewise C^1 maps defined in (4.16). It is by computing a large number of trajectories, each emanating from different values of x_0, that we are able to trace out the forms of these maps.

The nontrivial solutions for H_- that we seek correspond to trajectories emanating from particular equilibrium points in the far field, say $(x_0^*, 0, 0)$, that reach the near-field equilibrium point, $(A_-, 0, 0)$ for some finite $A_- \neq 0$. In addition to these nontrivial solutions, we recall that for all values of $m > 1$ there exists a trivial solution given by (4.13) with $n = 0$ that emanates from $x_0^* = x_Q = \sqrt{2/(m+1)}$ and reaches $A_- = 0$, as discussed in Proposition 4.3. Some representative results for $m = 2, 3, 4$, and 5 are shown in Figure 2. In these plots, a suitable nontrivial solution for H_- is found by identifying a value of $x_0 = x_0^*$ for which the value of $(\xi, u) = (A_-, 0)$—or $(\xi, w) = (A_-, 0)$—at the termination point.

In Figure 3, we show some representative computations highlighting the differences between the near-field behavior of trajectories local to a true solution with $A_- < 0$ and $A_- > 0$.

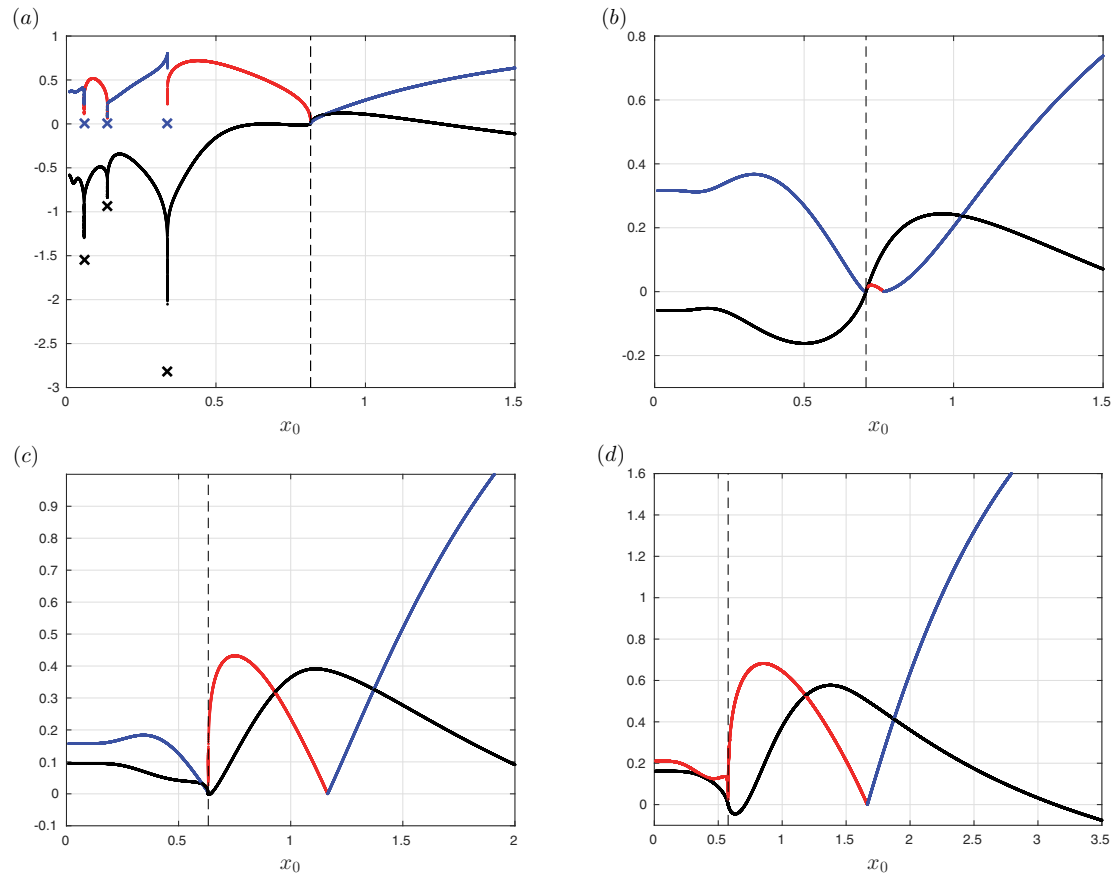

Figure 2. *Panels* (a)–(d) *show plots of the piecewise* C^1 *maps defined in* (4.16) *for* $m = 2, 3, 4,$ *and* 5, *respectively. In all cases the blue, red, and black curves show the value of* w *at* $u = 0$, *the value of* u *at* $w = 0$, *and the value of* ξ *at the termination point, respectively. The dashed vertical line indicates the value of* $x_0 = x_Q$ *corresponding to the exact solution* (1.17). *The crosses on panel* (a) *mark the data points extracted using the extrapolation procedure discussed in the text.*

As is evidenced by Figure 2, close to a trajectory with $A_- > 0$ the piecewise continuous C^1 maps defined in (4.16) are smooth, whereas close to a trajectory with $A_- < 0$ the maps exhibit rapid changes and (vertical) cusp-like features. As a result, determining negative value(s) of A_- is more challenging—despite resolving x_0 to machine precision (approximately 10^{-14} in the standard IEEE double precision), it is not possible to approximate the value of x_0^* sufficiently well that an accurate estimate of $A_-(< 0)$ can be determined. In these cases, we therefore found it necessary to implement one additional stage in the numerical scheme as follows.

Once x_0^* had been determined up to machine precision, and two "limiting" trajectories had been identified (one emanating from $x_0^* \pm \hat{\delta}$ and terminating at $u = 0$, and the other emanating from $x_0^* \mp \hat{\delta}$ and terminating at $w = 0$, where $\hat{\delta} \ll 1$) the expected near-field linear asymptotic behavior of $u(\xi)$, according to the expansion (1.14) with $n = 0$, is clearly visible. This linear behavior can then be extrapolated, in the direction of decreasing ξ, until it intersects the ξ-axis. This intersection point is, to a good approximation, the value of $A_-(< 0)$ corresponding

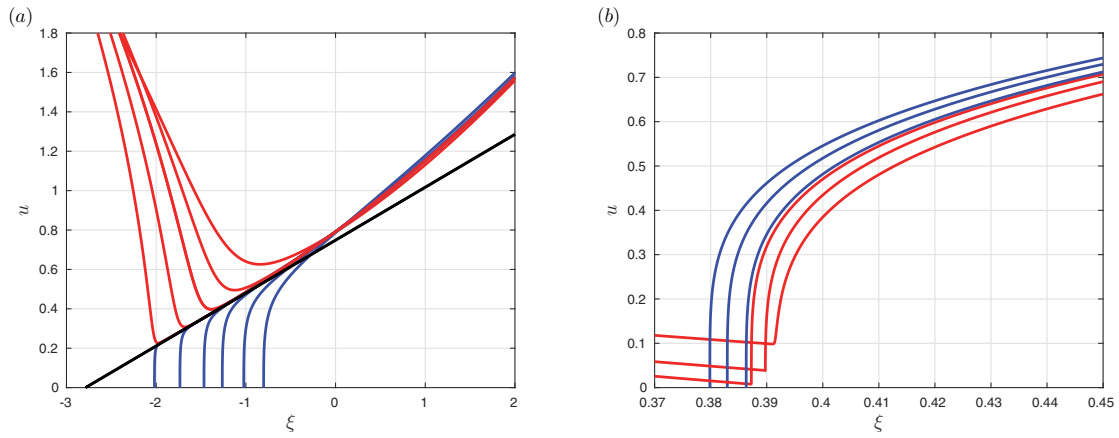

Figure 3. *Panel* (a) *shows some representative trajectories emanating from* $x_0^* \approx 0.338$ *for* $m = 2$. *More precisely, the red and blue trajectories begin at* $x_0^* \pm \hat{\delta}$ *for* $\hat{\delta} = 10^{-2}, 10^{-4}, 10^{-6}, 10^{-8}, 10^{-11}$, *and* 10^{-14}. *The black line shows the artificially extrapolated linear behavior. Panel* (b) *shows some representative trajectories emanating from* $x_0^* \approx 1.165$ *for* $m = 4$. *In this case, the trajectories begin at* $x_0^* \pm \hat{\delta}$ *for* $\hat{\delta} = 10^{-1}, 10^{-2}$, *and* 10^{-3}. *Notably, in the latter case, despite only resolving* x_0^* *to* 3 *significant digits, a good estimate of* A_- *has already been obtained.*

to the trajectory emanating from x_0^*. Panel (a) of Figure 3 gives an example of the linear extrapolation procedure described above.

Using the procedure described above, for all values of $m > 1$, we recover the trivial solution discussed in Proposition 4.3. In addition, we see that in the case $m = 3$ there is only one suitable nontrivial solution with the following data:

$$m = 3: \quad x_0^* \approx 0.767, \quad A_- \approx 0.129.$$

For $m = 4$ and $m = 5$, similar results are observed with one trivial and only one nontrivial solution as follows:

$$m = 4: \quad x_0^* \approx 1.165, \quad A_- \approx 0.386$$

and

$$m = 5: \quad x_0^* \approx 1.666, \quad A_- \approx 0.501.$$

In contrast, in the case $m = 2$ we find that three suitable nontrivial solutions exist with the data

$$m = 2: \quad \begin{cases} x_0^* \approx 0.338, & A_- \approx -2.804, \\ x_0^* \approx 0.137, & A_- \approx -0.932, \\ x_0^* \approx 0.0592, & A_- \approx -0.546. \end{cases}$$

Notably, all values of A_- for $m = 2$ are negative, whereas for $m = 3, 4$, and 5 they are positive.

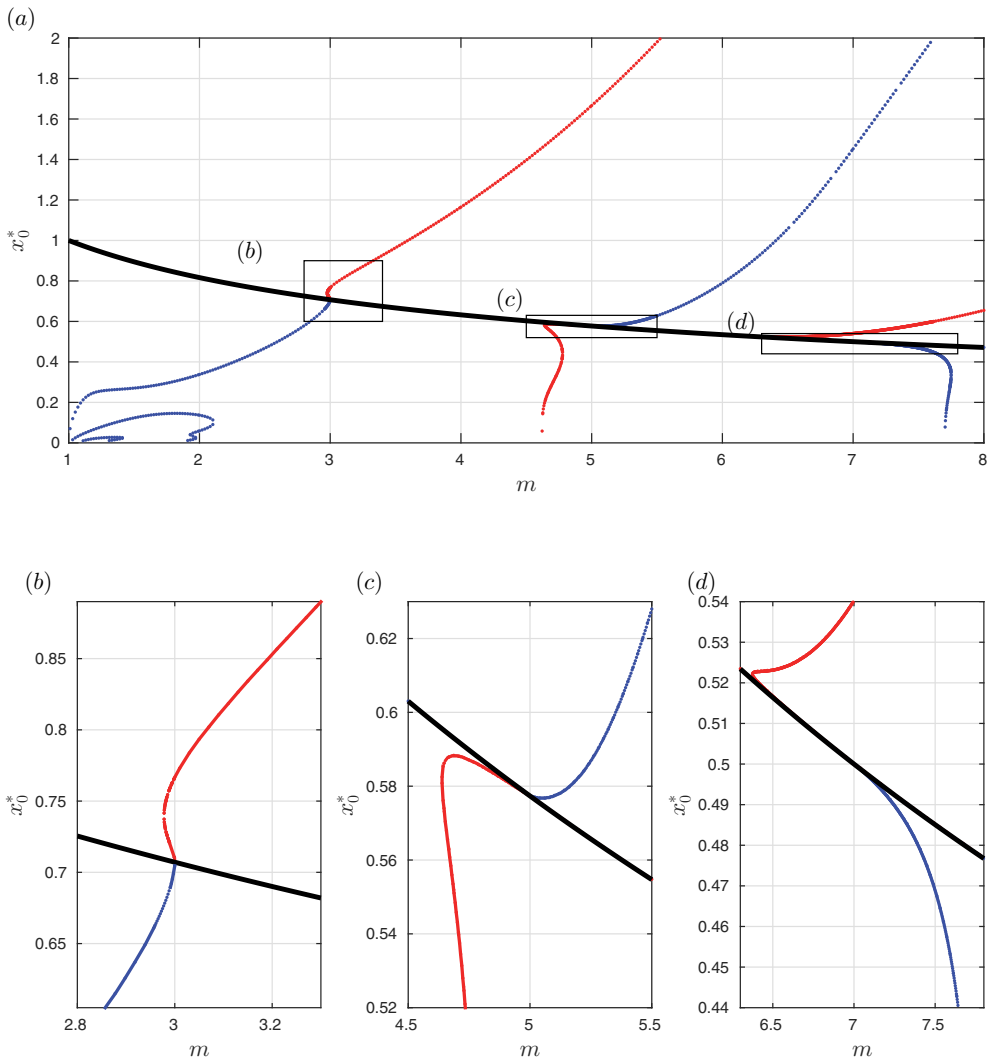

Figure 4. *The variation of x_0^* versus m. The red, blue, and black curves indicates values of x_0^* that define trajectories terminating at the near-field equilibrium point with $A_- > 0$, $A_- < 0$, and $A_- = 0$, respectively. Panels* (b)–(d) *show zoomed-in regions from panel* (a) *near $m = 3$, $m = 5$, and $m = 7$, respectively.*

In addition to the detailed results for $m = 2$, 3, 4, and 5 shown in Figure 2, we also show in Figure 4 the values of x_0^* determined for all values of m from $m = 1$ to $m = 8$. For the primary red and blue branches, emanating from $m = 3$ along the black branch, we show the corresponding values of A_- in Figure 5. Intriguingly, the numerical results indicate that in addition to the exact solution—which is valid for all $m > 1$—there are a whole host of additional solutions, some with $A_- > 0$ and others with $A_- < 0$. In particular, there is at least one additional trajectory corresponding to a suitable solution for H_- with $A_- > 0$ for all values of $m \gtrsim 2.978$. Further, for all $m < 3$ there exists at least one additional solution for

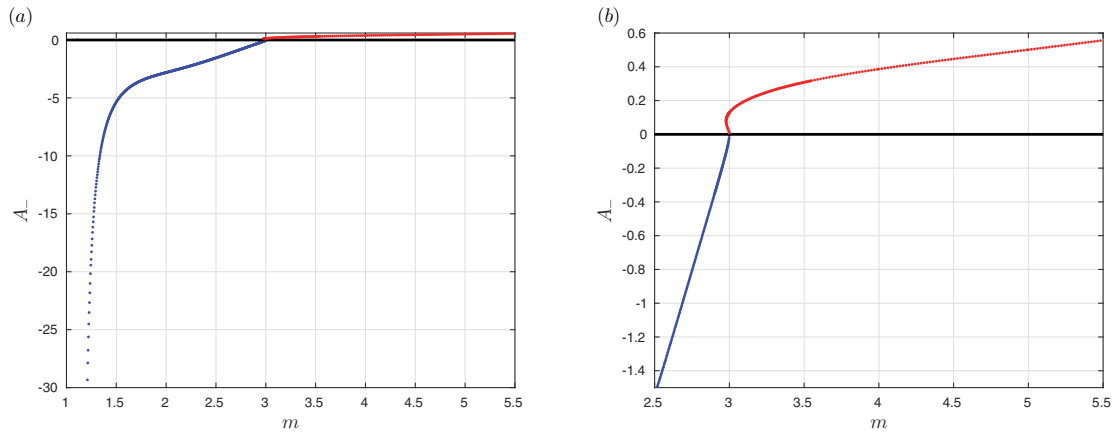

Figure 5. *Panel* (a) *shows the variation of* A_- *along the red and blue curves emanating from the black curve near* $m = 3$. *Panel* (b) *shows the same plot zoomed in on positive values of* A_-.

H_-, although, in this case, for a value of $A_- < 0$. Another noteworthy feature of the plots shown in panels (a)–(d) of Figure 4 is that at each value of $m = (2N-1)$ for $N \in \mathbb{N}$ additional branches of solutions depart from the black branch.

5.2. Solutions for $H_+(t > 0)$. Having successfully found suitable solutions for H_-, we now proceed to compute suitable solutions for H_+. As discussed in section 4.1, we can numerically construct a unique trajectory from small to infinite values of H_+. To do so, we integrate the system (2.4) from the equilibrium point $(A_+, 0, 0)$ in the near field towards the equilibrium point $(x_0, 0, 0)$ of the system (3.7) in the far field. The numerical procedure is carried out as follows:

1. Select a value of $A_+ \in \mathbb{R}\backslash\{0\}$. Since $(A_+, 0, 0)$ is an equilibrium point, it is not possible to escape $(A_+, 0, 0)$ in finite time. We therefore begin integration of the system (2.4) by taking a small step, say ϵ, away from $(A_+, 0, 0)$ using the relevant asymptotic behavior. Using (2.5) and (2.7) with $n = 0$ for $A_+ > 0$, we find that a trajectory exiting the equilibrium point along the center manifold, $W_c(A_+, 0, 0)$, has the local asymptotic behavior

$$\text{(5.2)} \qquad \begin{cases} \xi = A_+ + \epsilon, \\ u = \left(\frac{m+1}{2} A_+\right)^{-1} \epsilon + \mathcal{O}(\epsilon^2), & \text{for} \quad A_+ > 0, \\ w = \left(\frac{m+1}{2} A_+\right)^{-(m+1)} \epsilon^m + \mathcal{O}(\epsilon^{\min\{m+1, 2m-1\}}) \end{cases}$$

for a small positive value of ϵ. By contrast, using (2.11) and (2.12) with $n = 0$ for $A_+ < 0$, we find that a trajectory along the unstable manifold $W_u(A_+, 0, 0)$ has the local asymptotic behavior

$$\text{(5.3)} \qquad \begin{cases} \xi = -|A_+| + \epsilon, \\ u = \left(\frac{m+1}{2} |A_+| m\right)^{\frac{1}{m}} \epsilon^{\frac{1}{m}} + \mathcal{O}(\epsilon), & \text{for} \quad A_+ < 0, \\ w = \frac{1}{m} \left(\frac{m+1}{2} |A_+| m\right)^{\frac{m+1}{m}} \epsilon^{\frac{1}{m}} + \mathcal{O}(\epsilon) \end{cases}$$

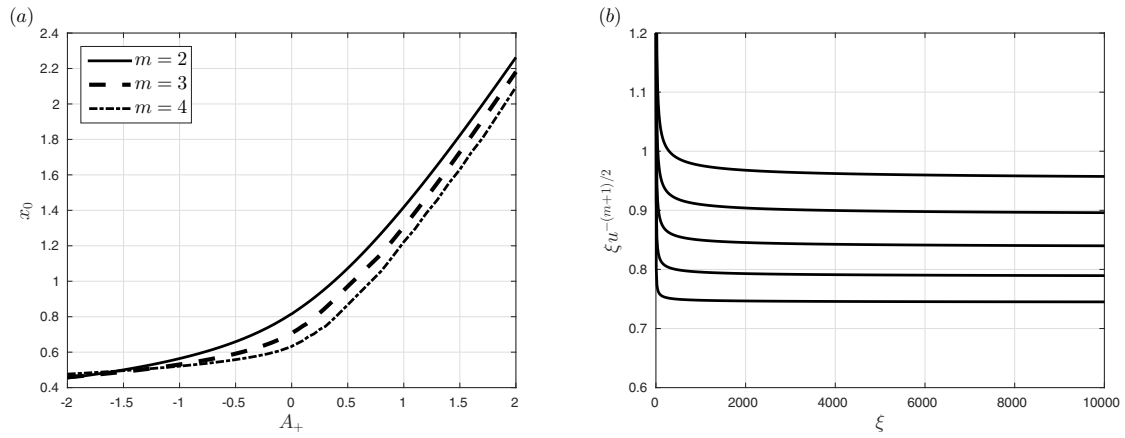

Figure 6. *Panel* (a): *Plots of the variation of* x_0 *with* A_+ *for various different values of* $m = 2$, 3, *and* 4. *Panel* (b): *Plots of the trajectories emanating from* $A_+ = 0.1$, 0.2, 0.3, 0.4, *and* 0.5 *for* $m = 3$. *The constant to which these trajectories tend in the far field is selected to be the corresponding value of* x_0.

for a small positive value of ϵ. Having selected values for both A_+ and ϵ, either (5.2) or (5.3) define unique (pseudo)initial conditions to begin integrating the system (2.4) in the direction of increasing time τ towards the far field.

2. We proved in Corollary 4.2, that the ultimate fate of all such trajectories, in variables (x, y, z), is approaching the equilibrium state $(x_0, 0, 0)$ for some $x_0 \in [0, \infty)$. Thus, by continuing integration of the system (2.4) with $n = 0$ to some large value of τ, denoted by say τ_∞, and reading off the value $\xi u^{-(m+1)/2} \approx x_0$ at $\tau = \tau_\infty$, we can obtain an arbitrarily accurate approximation of the corresponding value of x_0 that is obtained in the far field—a higher degree of accuracy can be achieved by simply increasing the value of τ_∞. For this purpose we found `ode45` with the majority of the default setting to be sufficiently robust. To ensure high numerical accuracy, at the cost of a relatively small increase in computation time, both `AbsTol` and `RelTol` were decreased to 10^{-10}. In contrast to the case for solutions H_-, we found it unnecessary to switch from integrating the near-field system (2.4) to the far-field system (3.7). Typically, we found that taking $\tau_\infty \in (10^4, 10^5)$ gave an approximation of x_0 correct to 8 significant digits.

Carrying out this procedure for a variety of choices of A_+ we are able to trace out the form of the piecewise C^1 map between A_+ and x_0 defined earlier in (4.8). In Figure 6, we show this map for $m = 2$, 3, and 4 (see panel (a)), as well as some representative trajectories of the system (2.4) for $m = 3$ (see panel (b)). In addition to the results shown, other computations for different values of m were also carried out and it appears generic that x_0 is a monotonically increasing function of A_+. Crucially, it appears that range of the map (4.8) is the entire semi-axis $\mathbb{R}^+$ for x_0.

5.3. Summary of numerical results for the self-similar solutions. We have demonstrated that (i) for each value of $m > 1$ and $n = 0$, there exists *at least* one value of $x_0 = x_0^*$ (different from the trivial case $x_0 = x_Q$) that defines a trajectory emanating from $(x_0^*, 0, 0)$ and terminating at $(A_-, 0, 0)$, and thus a suitable solution for H_-, and (ii) for every value of

$A_+ \in \mathbb{R}$ there exists a unique corresponding value of x_0, thereby defining an infinite family of suitable solutions for H_+. The one remaining step is therefore to invoke the matching condition (1.12). This condition is equivalent to requiring that the far-field behavior of H_+ is characterized by $x_0 = x_0^*$. Thus, given a solution for H_-, the matching condition (1.12) specifies a unique choice of $x_0 = x_0^*$, a unique A_+, and thus a unique solution for H_+, thereby closing the problem.

The solutions found here for $m = 3$ and 4 show a qualitative, although not quantitative, agreement with those reported in [6]. Here, we found that

$$m = 3: \quad A_- \approx 0.129, \quad A_+ \approx 0.154, \quad \text{and} \quad x_0^* \approx 0.767 \tag{5.4}$$

and

$$m = 4: \quad A_- \approx 0.386, \quad A_+ \approx 0.794, \quad \text{and} \quad x_0^* \approx 1.165. \tag{5.5}$$

In Foster et al. [6], they claimed that for $m = 3$: $A_- \approx 0.144$, $A_+ \approx 0.0958$, and $x_0^* \approx 0.765$, whereas for $m = 4$: $A_- \approx 0.386$, $A_+ \approx 0.341$, and $x_0^* \approx 0.980$. Additionally, they claim another suitable solution for $m = 2$: $A_- \approx 0.00135$, $A_+ \approx 0.0102$, and $x_0^* \approx 0.817$. In contrast, here we found that no such solution with $A_- > 0$ exists. Notably this value of x_0^* reported in [6] for $m = 2$ is very close to the value of $x_Q = \sqrt{2/(m+1)}$. For $m = 2$, using our numerical approach we have been able to identify three other solutions with $A_- < 0$, namely,

$$m = 2: \quad \begin{cases} A_- \approx -2.804, & A_+ \approx -4.322, & x_0^* \approx 0.338, \\ A_- \approx -0.932, & A_+ \approx -30.625, & x_0^* \approx 0.137, \\ A_- \approx -0.546, & A_+ \approx -166.623, & x_0^* \approx 0.0592. \end{cases} \tag{5.6}$$

We believe that the origin of these discrepancies is due to the low accuracy of the numerical scheme used in [6]. Indeed, in [6], the solutions for H_- were computed by identifying the value of A_- which characterizes solutions in the near field that extend into the far field with the requisite behavior, as in panel (a) of Figure 1. Solutions for H_+ were computed by finding the value of A_+ inferred (via shooting from the far field toward the near field) by invoking the matching condition in the far field as in panel (b) on Figure 6. Both numerical methods used in [6] are ill posed. Here, we pose the numerical problem as a shooting scheme for uniquely defined piecewise C^1 scalar functions, i.e., the maps defined in (4.8) and (4.16). We therefore believe that the results obtained here are more reliable than those in [6].

6. Numerical simulations of the time-dependent equation. Here we provide additional numerical evidence on the relevance of the self-similar solutions constructed in section 5 to the dynamics of the original time-dependent slow diffusion equation (1.1) with constant absorption ($n = 0$). In the interests of simplicity, we focus our interest on solutions to (1.1) that exhibit symmetry in space. This allows us to consider just a single moving interface located at $x = \ell(t) \leq 0$ while a Neumann (symmetry) condition will be imposed at $x = 0$. A complete definition of the problem we aim to solve is given by (1.1) subject to (1.3), $h|_{x=\ell(t)} = 0$, $\partial h/\partial x|_{x=0} = 0$, and supplemented with the initial condition $h|_{t=0} = h_0(x)$. Since we are primarily concerned with demonstrating stability of the self-similar solutions, we will focus on predicting the evolution of solutions as a reversing event is approached. Continuation of

a simulation past a reversing event can also be achieved using similar ideas to those that we will present, but a full discussion is beyond the scope of this work.

We shall design a numerical scheme based on finite difference approximations of the spatial derivatives and an adaptive Runge–Kutta–Fehlberg (RKF45) scheme for temporal evolution. The two main difficulties that this scheme must overcome are (i) dealing with the free boundary nature of the problem and (ii) the large gradients in the solution profiles that can develop close to the moving interface(s). The former issue will be circumvented by using a standard change of variables to map the problem to a static domain. A remedy for the latter issue will also be possible, but only after examining the possible behaviors of solutions to (1.1) local to an interface.

It is well known, and can be readily verified, that the nonlinear diffusion equation with absorption, (1.1), admits two different traveling wave solutions local to moving interfaces. Seeking solutions near a left interface $x = \ell(t)$ that have the form $h(x,t) \sim A(t)(x - \ell(t))^\alpha$, for some function $A(t)$ and constant α, we find that

$$h \sim (-m\ell'(t))^{1/m}(x - \ell(t))^{1/m} \quad \text{as} \quad x \searrow \ell(t) \quad \text{for} \quad \ell'(t) < 0, \tag{6.1}$$

$$h \sim \left(\frac{\ell'(t)}{1-n}\right)^{-1/(1-n)} (x - \ell(t))^{1/(1-n)} \quad \text{as} \quad x \searrow \ell(t) \quad \text{for} \quad \ell'(t) > 0. \tag{6.2}$$

The former is an advancing wave local to a left interface whose motion is driven by diffusion, whereas the latter is a receding wave driven by absorption. The study of self-similar solutions has elucidated a process by which the wave (6.1) *becomes* (6.2), giving rise to a reversing interface, or vice versa, giving rise to an antireversing interface. Notably, for $m > 0$ the behavior (6.1) exhibits extremely large gradients close to the interface. The same large gradients are observed in (6.2) when $n < 0$. Any finite difference scheme that attempts to accurately capture these large gradients will be susceptible to roundoff error and therefore lead to inaccuracy. However, knowledge of these forms of the local behaviors, (6.1) and (6.2), can be used to motivate a change of variables that "regularizes" the behavior of solutions local to the interface so that a finite-difference-based approach can yield reliable results.

To remove the issues associated with the free boundary nature of the problem we first make the change of variables

$$\mu = \frac{x}{\ell(t)}, \tag{6.3}$$

so that the domain of interest is now $\mu \in [0,1]$. Since our primary aim here is to demonstrate the stability of the self-similar solutions in the context of the original PDE (1.1) we will concentrate on evolving some initial data forwards in time towards a reversing event. With this in mind, we expect that for suitable choices of initial data the local behavior near the left interface ($x = \ell$ or equivalently $\mu = 1$) will be given by (6.1). This local behavior motivates the following change of variables:

$$\nu = (1 - \mu)^{1/m}, \tag{6.4}$$

where $\nu \in [0,1]$. Following the transformations (6.3) and (6.4), the original PDF (1.1) with

$n = 0$, and its associated boundary conditions become

$$\frac{\partial \hat{h}}{\partial \hat{t}} = \frac{1}{m^2 \ell^2 \nu^{m-1}} \frac{d}{d\nu} \left(\frac{\hat{h}^m}{\nu^{m-1}} \frac{\partial \hat{h}}{\partial \nu} \right) - \frac{d\ell}{d\hat{t}} \frac{(1-\nu)^m}{m\ell\nu^{m-1}} \frac{\partial \hat{h}}{\partial \nu} - 1, \tag{6.5}$$

$$\left. \frac{\partial \hat{h}}{\partial \nu} \right|_{\nu=1} = 0, \qquad \hat{h}|_{\nu=0} = 0, \tag{6.6}$$

$$\frac{d\ell}{d\hat{t}} = \frac{\hat{h}^{m-1}}{m\ell\nu^{m-1}} \left. \frac{\partial \hat{h}}{\partial \nu} \right|_{\nu=0^+}, \tag{6.7}$$

where $\hat{h}(\nu, \hat{t}) = h(x, t)$. Note that (6.7) arises from (1.3) under the assumption that $\ell' < 0$. At this stage it is now obvious why the change of variables (6.4) is so crucial to the success of a finite-difference-type treatment of the problem; the singular behavior (6.1) has been fully removed, and replaced with a linear behavior (in the ν-coordinate system for $\hat{h}$) which can readily captured by finite differences. The one remaining issue with the problem (6.5)–(6.7) that must be resolved before we proceed to discretization concerns accurately evaulating the right-hand side of the evolution equation for ℓ, namely, (6.7). Once again, we exploit our knowledge of the linear behavior of the solution profile local to the moving interface, near $\nu = 0$, to write the following generic Taylor expansion $\hat{h}|_{\nu=0} = (\partial \hat{h}/\partial \nu|_{\nu=0^+})\nu + \mathcal{O}(\nu^2)$. On substitution of this expansion into (6.7) we find that

$$\frac{d\ell}{d\hat{t}} = \frac{1}{m\ell} \left(\frac{\partial \hat{h}}{\partial \nu} \right)^m \Big|_{\nu=0^+} + \mathcal{O}(\nu). \tag{6.8}$$

We henceforth truncate the above approximation immediately after the leading order term.

6.1. Finite difference discretization. The spatial domain is treated by introducing a uniformly spaced discretization consisting of $N+1$ grid points located at $\nu_i = (i-1)/N$ for $i \in 1, 2, \ldots, N+1$. At each of these stations in space we denote the value of the concentration by $\hat{h}_i(\hat{t}) = \hat{h}|_{\nu=\nu_i}$. A system of $N+1$ evolution equations for the values of the independent variable, $\hat{h}|_{\nu=\nu_i}$, along with one additional ODE for the position of the interface, ℓ, may now be formed by using finite differences to discretize (6.5) and (6.8) along with the boundary conditions (6.6). On doing so, and using concise notation, the resulting problem may be written as

$$\frac{d\mathbf{u}}{d\hat{t}} = \mathbf{f}(\mathbf{u}) \quad \text{with} \quad \mathbf{u}|_{\hat{t}=0} = \mathbf{u}_0. \tag{6.9}$$

Here, the solution vector $\mathbf{u}$ is a vector of length $N+2$ comprised of the functions $\hat{h}_i(\hat{t})$ and $\ell(\hat{t})$ while the initial data vector $\mathbf{u}_0$ contains the initial values of these same quantities, and the nonlinear operator $\mathbf{f}$ is the operator arising from the finite difference discretization of the problem. In the interests of brevity we will not explicitly show the operator $\mathbf{f}$. However, it is pertinent to note that for the purposes of this work we formed $\mathbf{f}$ by treating each and every first derivative in space appearing in (6.5) using a second-order accurate centered difference

while the first derivatives in space appearing in (6.6) and (6.8) were treated using second-order accurate backward and forward differences, respectively.

The system of ODEs and initial data (6.9) can then be evolved in time using an appropriate time stepping method. For convenience, we used the MATLAB routine `ode45` which implements an RKF45 scheme. The `Events` function was used to automatically detect when the solution approached a reversing event by monitoring the value of ℓ' and stopping the temporal integration when $|\ell'| < \bar{\delta}$ for some $\bar{\delta} \ll 1$.

For all of the simulations shown here we found that selecting the number of grid points $N = 10^3$, taking $\bar{\delta} = 10^{-10}$, and setting `AbsTol` and `RelTol`, in the `ode45` solver, both equal to 10^{-10} gave accurate results. In addition to the usual convergence tests we verified the validity of the approach by monitoring the "total mass" of the concentration. On taking the original PDE, (1.1) with $n = 0$, integrating over the spatial domain and applying the Neumann and interface conditions at $x = 0$ and $x = \ell(t)$, respectively, one can show that solutions to the problem should satisfy $d/dt(\int_\ell^0 h(x,t)dx) = -\ell$. Rewriting this equation under the changes of variables (6.3) and (6.4) gives rise to

$$\frac{d}{d\hat{t}}\left(m\ell \int_0^1 \nu^{m-1}\hat{h}d\nu\right) + \ell = 0. \tag{6.10}$$

The numerical scheme was found to reproduce this result up to the expected numerical error. As either N was increased or `AbsTol` and `RelTol` were decreased the discrepancies between (6.10) and the numerical results decreased at the expected rates—in summary, the method was found to perform as expected.

6.2. Summary of numerical results for the time-dependent equation. To provide evidence for the stability of the self-similar solutions found in section 5 in the context of the original PDE problem (1.1) we will examine the evolution of the following one-parameter family of initial conditions

$$\hat{h}|_{\hat{t}=0} = \hat{h}_0 = \lambda \sin\left(\frac{\pi\nu}{2}\right) \quad \text{and} \quad \ell|_{\hat{t}=0} = \ell_0, \tag{6.11}$$

for a selection of values of $\lambda \in \mathbb{R}^+$. Owing to the linear behavior of (6.11) close to $\nu = 0$ we expect to, and indeed do, find that $\ell' < 0$ initially. We evolve the system until a reversing event is approached and then simulation is terminated.

Panel (a) of Figure 7 shows plots of the behavior of $\ell(t)$ as the reversing event is approached as predicted by (i) direct numerical simulation, and (ii) the self-similar theory, for the choice of the exponent $m = 4$ and $n = 0$. One can see that independently of the choice of λ in the initial data (6.11), the agreement betweeen the two approaches is very favorable. Other similar simulations were carried out for a variety of different choices of $3 \le m \le 5$ and for different initial data and good agreement was observed in all cases thereby providing strong evidence that the self-similar reversing solutions are stable in the time-dependent context. In addition to this comparison of the predictions on the behavior of ℓ we also show, in Figure 7 panel (b), a series of plots of $h(x,t)$ at different times as predicted by the numerical simulation;

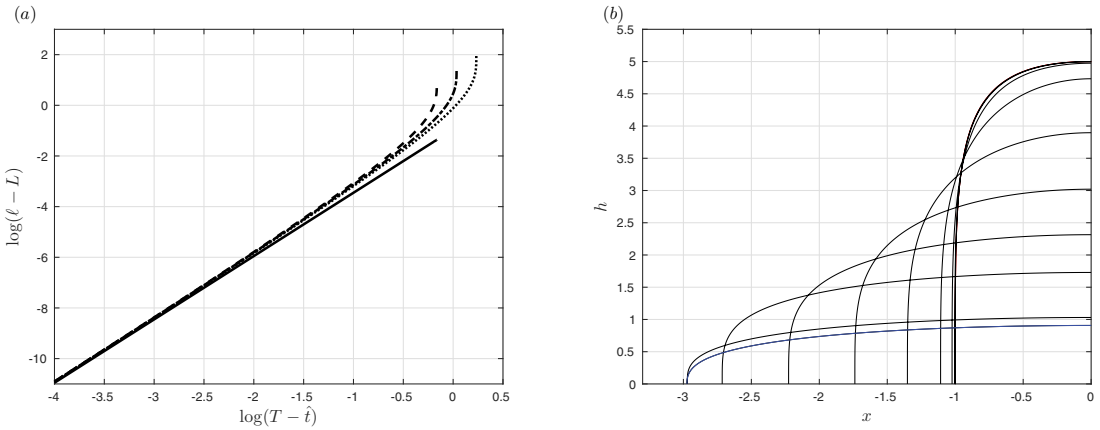

Figure 7. *Panel* (a) *shows a comparison between the predictions on the behavior of* $\ell(t)$ *as given by* (i) *the self-similar theory (solid line), i.e., according to* (1.13) *and* (5.5), *and* (ii) *direct numerical simulation for* $m = 4$ *and* $n = 0$. *The dashed, dash-dotted, and dotted curves show the results from direct numerical simulation using the initial data* (6.11) *with* $\lambda = 5, 10, 20$, *respectively, and* $\ell_0 = 1$. *The quantities* T *and* L *on the horizontal and vertical axes denote the values of* t *and* ℓ *at which the simulation was terminated. Panel* (b) *shows representative plots of* $h(x,t)$ *for the choice* $\lambda = 5$ *at* 10 *equally spaced values of* t. *The blue curve show the solution immediately prior to the reversing event, i.e., when the simulation was terminated.*

one can see that the expected large gradients near the moving interface have been manifested and captured by the scheme.

7. Conclusion. This work has focused on constructing local (in both space and time) self-similar reversing and antireversing solutions to the nonlinear diffusion equation (1.1) with $m > 0$, $n < 1$, and $m + n > 1$. We have demonstrated how the dynamical theory combined with a numerical scheme can be used to furnish suitable solutions to the differential equations (1.8) for H_- and H_+. Via the self-similar reductions (1.7), the solutions to these differential equations can be transformed into physically meaningful solutions for $h(x,t)$ to the nonlinear diffusion equation (1.1), which is completed with the no flux boundary condition (1.3) and the condition $h|_{x=\ell(t)} = 0$. The stability of these local solutions in the time-dependent context of the original equation has been validated against direct numerical simulation of (1.1).

Let us now summarize the main technique developed in this paper. In section 5.1 we used the result of Lemma 4.4 to numerically construct suitable solutions for H_-. For $n = 0$ and each value of $m > 1$, we identified *at least* one suitable solution, defined by a pair of values of A_- and x_0^*, in addition to the exact solution (1.17)—in the original time and space variables, this exact solution corresponds to a steady solution for $h(x,t)$ and thus does not constitute a reversing or an antireversing solution. In section 5.2, we used Lemma 4.1 to formulate a numerical scheme for constructing solutions for H_+ defined by pairs of values of A_+ and x_0^*. We showed that the map (4.8) is one-to-one and its range is the entire semiaxis $\mathbb{R}^+$ for x_0. For each value of $m > 1$, we found that (i) if $A_+ < 0$ then $x_0 < x_Q$, and (ii) if $A_+ > 0$ then $x_0 > x_Q$, where $x_Q = \sqrt{2/(m+1)}$. The final stage in constructing solutions for $h(x,t)$ is to invoke the matching condition (1.12) that ensures continuity of $h(x,t)$ across $t = 0$. In summary we have found that for $1 < m < 3$, up to 5 different solutions are available with

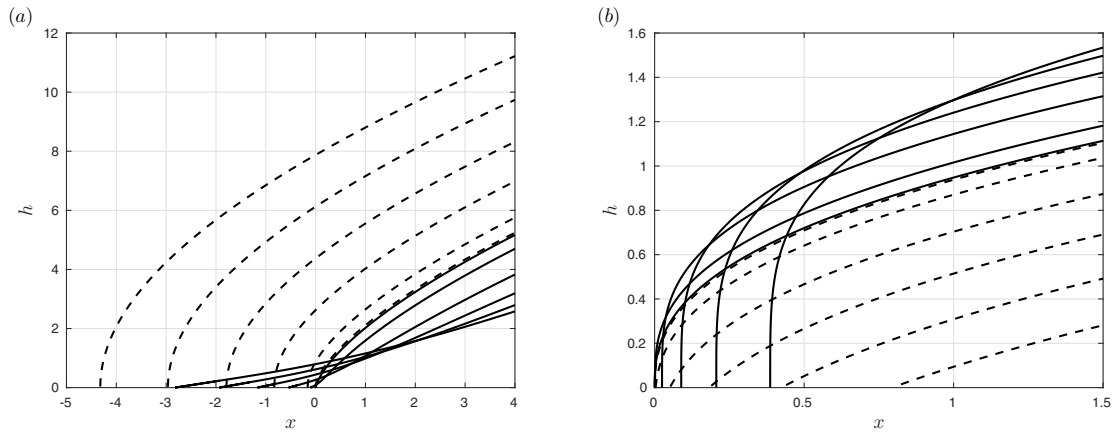

Figure 8. *Representative plots of $h(x,t)$ at 10 equally spaced values of t between -1 and 1, and for $t = \pm 10^{-3}$ to demonstrate the continuity of $h(x,t)$ across $t = 0$. Solid and dashed curves show the solution for $t < 0$ and $t > 0$, respectively. Panel* (a) *shows the antireversing dynamics for $m = 2$ and $n = 0$, $A_- \approx -2.804$, $A_+ \approx -4.322$, and $x_0^* \approx 0.338$. Panel* (b) *shows the reversing dynamics for $m = 4$ and $n = 0$, $A_- \approx 0.386$, $A_+ \approx 0.794$, and $x_0^* \approx 1.165$.*

$A_-, A_+ < 0$. For $m \gtrsim 2.9$ there is at least one solution with $A_-, A_+ > 0$. When $5 > m \gtrsim 4.6$ there is at least one solution with $A_- > 0$ and $A_+ < 0$. When $m > 5$ solutions with $A_- < 0$ and $A_+ > 0$ are available. For $7.75 \gtrsim m > 7$ an additional branch of solutions with $A_-, A_+ < 0$ emerges, whereas for $m \gtrsim 6.42$, there is another branch of solutions with $A_-, A_+ > 0$. For $m > 8$ it seems quite possible that yet more branches of solutions will emerge.

There are distinct differences between the interpretation of solutions with (i) $A_-, A_+ > 0$, (ii) $A_-, A_+ < 0$, (iii) $A_- > 0$ and $A_+ < 0$, and (iv) $A_- < 0$ and $A_+ > 0$, in terms of the original time-dependent model (1.1). Solutions of type (i) correspond to a reversing solution where the left interface advances for $t < 0$ with the behavior (6.1), and then subsequently recedes for $t > 0$ with the behavior (6.2). In contrast, solutions of type (ii) correspond to an antireversing solution where the interface recedes for $t < 0$ with the form (6.2), and then advances according to the form (6.1) for $t > 0$. One representative local solution for $h(x,t)$ for behaviors of type (i) and (ii)—one reversing and one antireversing—are shown in Figure 8. Solutions of type (iii) and (iv) are termed pausing advancing, and pausing receding solutions, respectively. Type (iii) solutions advance for $t < 0$, instantaneously stop at $t = 0$, and then continue advancing for $t > 0$ all with the behavior (6.1), whereas solutions of type (iv) recede for $t < 0$, pause at $t = 0$, and continue receding for $t > 0$ according to the behavior (6.2).

Some natural open questions raised by this study are (i) whether any self-similar solutions with nonmonotone profiles (in ξ) exist—i.e., solutions that do not satisfy (1.10), and (ii) if more than one reversing or antireversing solution is stable for a particular value of m, what is the mechanism for selecting the appropriate self-similar solution at a particular reversing or antireversing event.

Acknowledgments. J. F. thanks J. R. King, and A. D. Fitt, while D.P. thanks M. Chugunova and R. Taranets for useful discussions regarding this project. J. F. thanks B. Protas for hospitality and many useful discussions. A part of this work was completed during

the visit of D. P. to Claremont Graduate University. Generalization of invariant manifolds from the case of constant absorption ($n = 0$) to $n \neq 0$ was completed together with P. Gysberg during his undergraduate project.

REFERENCES

[1] J. M. Acton, H. E. Huppert, and M. G. Worster, *Two dimensional viscous gravity currents flowing over a deep porous medium*, J. Fluid Mech., 440 (2001), pp. 359–380.
[2] D. G. Aronson, *Regularity properties of flows through porous media*, SIAM J. Appl. Math., 17 (1969), pp. 461–467.
[3] X. Y. Chen, H. Matano, and M. Mimura, *Finite-point extinction and continuity of interfaces in a nonlinear diffusion equation with strong absorption*, J. Reine Angew. Math., 459 (1995), pp. 1–36.
[4] C. Chicone, *Ordinary Differential Equations with Applications*, 2nd ed., Texts Appl. Math. 34, Springer, New York, 2006.
[5] F. Dimortier, *Local study of planar vector fields: Singularities and their unfoldings*, in Structures in Dynamics: Finite-Dimensional Deterministic Studies, North Holland, Amsterdam, 1991, pp. 161–242.
[6] J. M. Foster, C. P. Please, A. D. Fitt, and G. Richardson, *The reversing of interfaces in slow diffusion processes with strong absorption*, SIAM J. Appl. Math., 72 (2012), pp. 144–162.
[7] J. M. Foster and A. D. Fitt, *The halting of cantact lines in slender viscous films driven by gravity and surface tension gradients*, Phys. Fluids, A26 (2014), 073601.
[8] V. A. Galaktionov, S. I. Shmarev, and J. L. Vazquez, *Regularity of interfaces in diffusion processes under the influence of strong absorption*, Arch. Ration. Mech. Anal., 149 (1999), pp. 183–212.
[9] M. L. Gandarias, *Classical point symmetries of a porous medium equation*, J. Phys. A., 29 (1994), pp. 607–633.
[10] M. E. Gurtin, *On the diffusion of biological populations*, Math. Biosci., 33 (1977), pp. 35–49.
[11] M. A. Herrero and J. L. Vázquez, *The one-dimensional nonlinear heat equation with absorption: Regularity of solutions and interfaces*, SIAM J. Math. Anal., 18 (1987), pp. 149–167.
[12] M. W. Hirsh, C. C. Pugh, and M. Shub, *Invariant Manifolds*, Lecture Notes in Math. 583, Springer, Berlin, 1977.
[13] A. S. Kalashnikov, *The propagation of disturbances in problems of nonlinear heat conduction with absorption*, USSR Comput. Math. Phys., 14 (1974), pp. 70–85.
[14] B. Kawohl and R. Kersner, *On degenerate diffusion with very strong absorption*, Math. Methods Appl. Sci., 15 (1992), pp. 469–477.
[15] R. Kersner, *Nonlinear heat conduction with absorption: Space localization and extinction in finite time*, SIAM J. Appl. Math., 43 (1983), pp. 1274–1285.
[16] D. Pritchard, A. W. Woods, and A. J. Hogg, *On the slow draining of a gravity current moving through a layered permeable medium*, J. Fluid Mech., 444 (2001), pp. 23–47.
[17] B. Sandstede and A. Scheel, *Evans function and blow-up methods in critical eigenvalue problems*, Discrete Contin. Dyn. Syst., 10 (2004), pp. 941–964.
[18] S. Wiggins, *Normally Hyperbolic Invariant Manifolds in Dynamical Systems*, Springer, New York, 1994.
[19] W. W. Zhang and J. R. Lister, *Similarity solutions for van der Waals rupture of a thin film on a solid substrate*, Phys. Fluids, A9 (1999), pp. 2454–2462.